Published in final edited form as:

Adv Drug Deliv Rev. 2017 April ; 113: 157–176. doi:10.1016/j.addr.2016.08.001.

Positron Emission Tomography and Nanotechnology: A Dynamic Duo for Cancer Theranostics

Shreya Goel[1], **Christopher G. England**[2], **Feng Chen**[3,*], and **Weibo Cai**[1,2,3,4,*]

[1]Materials Science Program, University of Wisconsin – Madison, Madison, WI 53705

[2]Department of Medical Physics, University of Wisconsin-Madison, Madison, WI 53705

[3]Department of Radiology, University of Wisconsin-Madison, Madison, WI 53792

[4]University of Wisconsin Carbone Cancer Center, Madison, WI 53792

Abstract

Development of novel imaging probes for cancer diagnosis is critical for early disease detection and management. The past two decades have witnessed a surge in the development and evolution of radiolabeled nanoparticles as a new frontier in personalized cancer nanomedicine. The dynamic synergism of positron emission tomography (PET) and nanotechnology combines the sensitivity and quantitative nature of PET with the multifunctionality and tunability of nanomaterials, which can help overcome certain key challenges in the field. In this review, we discuss the recent advances in radionanomedicine, exemplifying the ability to tailor the physicochemical properties of nanomaterials to achieve optimal *in vivo* pharmacokinetics and targeted molecular imaging in living subjects. Innovations in development of facile and robust radiolabeling strategies and biomedical applications of such radionanoprobes in cancer theranostics are highlighted. Imminent issues in clinical translation of radiolabeled nanomaterials are also discussed, with emphasis on multidisciplinary efforts needed to quickly move these promising agents from bench to bedside.

Graphical Abstract

[*]**Correspondence to:** F. Chen, Department of Radiology, University of Wisconsin – Madison, 1111 Highland Avenue, Madison, WI 53705, USA, chenf@mskcc.org, W. Cai, Departments of Radiology and Medical Physics, University of Wisconsin – Madison, 1111 Highland Avenue, Madison, WI 53705, USA, WCai@uwhealth.org.

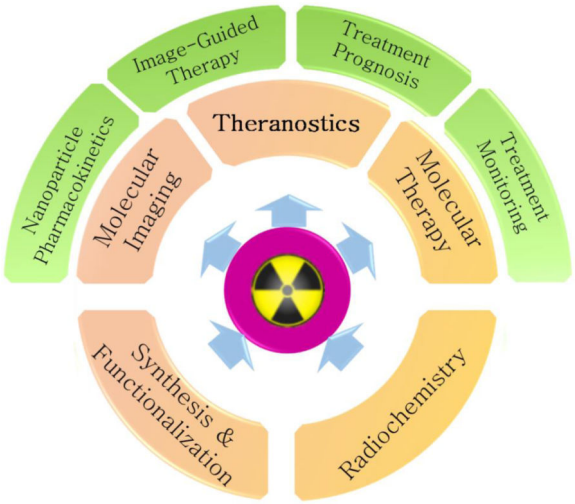

Keywords

Positron Emission Tomography; Nanotechnology; Cancer Theranostics; Radiochemistry; Radiolabeled Nanoparticles

1. Positron Emission Tomography in Molecular Imaging

Rapid development in the fields of cancer biology, genomics, proteomics and clinical oncology has revolutionized personalized cancer management through the integration of molecular and physiological information with the anatomic readouts obtained *via* conventional imaging modalities.[1] Defined as “non-invasive, real-time characterization and measurement of biological processes at the cellular and molecular level within living cells, tissues and intact subjects”, [2] molecular imaging promises enormous potential in the areas of diagnostics, therapy monitoring, drug discovery and development, and understanding nanoscale reactions such as protein-protein interactions and enzymatic conversion.[3, 4] Molecular imaging encompasses different modalities including optical bioluminescence, optical fluorescence (FL), targeted ultrasound, molecular magnetic resonance imaging (MRI) and spectroscopy (MRS), single-photon-emission computed tomography (SPECT), and positron emission tomography (PET).[1] The inherent strengths and limitations of each modality have spurred active development of multimodal systems, *e.g.* SPECT/CT, PET/CT, optical/CT and PET/MRI for synergistic imaging. Owing to their high detection sensitivity (10^{-11}–10^{-12} M), quantifiability, limitless depth of penetration, as well as advances in radiotracer development, non-invasive nuclear imaging modalities, SPECT and PET offer tremendous opportunities in early lesion detection, patient screening and stratification, and individualized treatment monitoring and dose optimization.[4, 5]

Since its inception in 1970s,[6] PET has emerged as a clinical modality of choice for staging and restaging of a variety of malignancies. PET requires internal administration of tracer quantities (usually nanomolar) of a radiolabeled pharmaceutical, specific and selective for a target of interest. The fate of the radiolabeled agent *in vivo* is tracked with a camera which

detects two coincident high energy gamma-rays (511 keV) emitted ~180° apart resulting from the annihilation of the emitted positron with a nearby electron.[7] While [^{18}F]fluorodeoxyglucose (FDG) remains the most widely used PET tracer (>95% of all clinical PET scans), PET has adopted different positron emitting radionuclides including Copper-61/64($^{61/64}$Cu, $t_{1/2}$: 3.3 h and 12.7 h), Gallium-66/68 ($^{66/68}$Ga, $t_{1/2}$: 9.5 and 1.1 h), Zirconium-89 (^{89}Zr, $t_{1/2}$: 78.4 h), and Iodine-124 (^{124}I, $t_{1/2}$: 100.2 h), among many others. FDG is a glucose analog that is selectively taken up by rapidly metabolizing cells, a hallmark of most malignancies, and has been clinically approved for staging of a number of cancers including breast, colorectal, esophageal, head and neck cancers, melanomas and lymphomas.[1] Since glucose metabolism is not specific only to cancer cells, imaging with FDG can be counter-productive in certain cases. This has fueled intense research for development of newer imaging agents such as antibodies and their fragments, small proteins and peptides and other biologically relevant entities, specifically targeted for a molecular event. Nanomaterials that combine different imaging modalities, targeting ligands and therapeutic moieties all in a single vector, have recently emerged as a new frontier in molecularly targeted probes.

2. Nanotechnology in Positron Emission Tomography: An Emerging Paradigm

The introduction of nanotechnology in nuclear imaging (mainly PET and SPECT) has generated much interest in the past decade.[8] Nanomaterials, typically smaller than a few hundred nanometers have emerged as forerunners in nanooncology, for targeted drug delivery, therapy and patient monitoring.[9] The biggest advantage that nanotechnology brings is to bridge the gap between the macroscopic and microscopic worlds, where nanomaterials prove to be the ideal medium for interfacing with the biological systems. Nanoparticles possess novel properties that distinguish them from bulk material: large functional surface area, easily controllable surface chemistry which facilitates binding to small molecule drugs, imaging labels and targeting ligands like antibodies, peptides, nucleic acids, *etc*. Moreover, their small size (~100– 10,000 times smaller than human cells) allows unique intracellular and extracellular interactions, such as extravasation through endothelial cells and enhanced permeability and retention (EPR) in tumor tissues.[4] Owing to the immense and unique possibilities it offers, nanotechnology has attracted significant investment from the National Institutes of Health (NIH)/National Cancer Institute (NCI) and some nanoparticles have also progressed into clinical trials.[10] For example, gold nanoparticles have found clinical applications towards head and neck cancer, as evidenced by recent completion of two first-in-human phase I clinical trials (AuNP-conjugated tissue necrosis factor (TNF) treatment in solid tumors [11] and AuNP-mediated hyperthermia for therapy of refractory and/or recurrent tumors of the head and neck).[10, 12] In addition, fluorescent silica nanoparticles (also known as C dots) are about to enter phase II clinical trials for lymph node mapping in head and neck melanoma, breast and cervical/uterine cancer patients.[13] Although much work is still required in understanding the long-term toxicities and optimal applications of nanomaterials in human subjects, these studies demonstrate the paradigm-shifting revolution that nanotechnology can bring in advancement of cancer prevention, diagnosis, treatment and management.

The role of nanotechnology in molecular imaging is four-fold. Nanoparticles can act as signal amplifiers, resulting in higher contrast indices and enhanced sensitivity. The large surface area can be functionalized with different targeting moieties, creating a multifunctional nanoplatform for targeted detection of different diseases. A big advantage of using nanoprobes over the traditional biological moieties is the competence for multimodality. Besides radiolabeling for PET, most nanoparticles possess intrinsic properties that can be easily harnessed for other molecular imaging modalities. For example radiolabeled iron oxide nanoparticles (IONPs) simultaneously signal for both MRI and PET; the generated data can potentially overcome the limitations of individual modality. The final advantage lies in the ability to combine both diagnostic and therapeutic capabilities onto the same vector, giving rise to the concept of theranostics.

The union of PET and nanotechnology represents a symbiotic relationship, promising mutual benefits for each. On one hand, the unique physicochemical properties and multivalency of nanomaterials promise unprecedented applications in molecular PET; noninvasive interpretation of biological events, synergistic multimodal imaging (such as PET/CT, PET/MR, and PET/US) and theranostics. On the other hand, PET has emerged as a formidable tool in the biomedical applications of nanomaterials for cancer theranostics. For example, it is widely known that the physicochemical properties of nanoparticles such as size, shape, surface charge and chemistry (PEGylation, ligand conjugation), and composition affect their *in vivo* biodistribution.[14, 15] Efforts are being undertaken to understand and optimize the factors influencing the pharmacokinetics, intratumoral penetration, tumor bioavailability, and cargo delivery mechanisms of nanoparticulate agents. In this regard, the sensitivity, whole body imaging capability, non-invasive and quantitative nature of PET makes it an excellent choice for accurately exploring the complex biological pathways and *in vivo* ADME (Absorption, Distribution, Metabolism and Excretion) profiles of nanoparticles, which have been the major roadblocks in clinical translation of nanomaterials. Secondly, PET has been exploited in image-guided therapy and drug delivery applications of nanomaterials, which allow real-time monitoring of the therapeutic outcomes.[16–18] Moreover, nanoparticles radiolabeled with positron emitters can potentially be employed in treatment prognosis and patient selection, aptly demonstrated in a recent study using ^{89}Zr-labeled nanoreporter for Doxil.[19] Co-injection of the nanoreporter with the clinically approved anti-cancer nanodrug Doxil was able to predict the therapeutic outcomes based on the tumor uptake in a murine breast cancer model. While still in preclinical settings, such systems hold promise for clinically relevant cancer management in the future.

3. Development of Radiolabeled Nanoparticles

The radiostability of the isotope: nanoparticle complex is integral to the correct interpretation of *in vivo* biodistribution data, and thus, development of radiolabeled nanoplatforms is a non-trivial issue and warrants careful thought. Successful design of a radiolabeled nanoprobe involves rational selection of the isotope, the radiolabeling strategy and the nanoplatform; carefully tuned to achieve the highest radiochemical yields and stability, as well as optimal *in vivo* biodistribution and imaging contrast. Selection of an appropriate radioisotope depends on its imaging characteristics, decay half-life, chelation chemistry and availability. Ideally, isotopes with low positron energy and high β^+ branching

ratio are favorable for PET imaging. Based on their half-lives, positron emitting isotopes can be either short-lived (e.g. ^{11}C; $t_{1/2}$ = 20 min, ^{15}O; $t_{1/2}$ = 2 min, ^{18}F; $t_{1/2}$ = 109.7min, ^{68}Ga; $t_{1/2}$ = 67.7 min and so on) or longer-lived (^{72}As; $t_{1/2}$ = 26 h, ^{89}Zr; $t_{1/2}$ = 3.2 d and ^{124}I; $t_{1/2}$ = 4.2 d). Matching the decay half-life with the biological half-life of the tracer is another important aspect, especially for nanomaterials with prolonged circulation *in vivo*.

Complexation of the radionuclide and the nanoparticle is an important aspect in the development of a successful radiotracer. Ideally, a radiolabeling method must be robust, quick, safe, and highly efficient with minimal effect on the intrinsic pharmacokinetics of the vector.[20] There are five major radiolabeling strategies, each with their advantages and disadvantages; their selection determined by the isotope and nanoparticle chosen for the imaging purpose (Figure 1). Traditional method involves tethering of the radiometals to the nanoplatform *via* chelators such as 1,4,7-triazacyclononane-1,4,7-triacetic acid (NOTA), 1,4,7,10-tetraazacyclododecane-1,4,7,10-tetraacetic acid (DOTA), p-isothiocyanatobenzyl-desferrioxamine (Df-Bz-NCS), diethylene triamine pentaacetic acid (DTPA), *etc. via* specific coordination chemistry. Since the nanoparticle itself is not radiolabeled, potential detachment of the radiometal containing chelator or polymer coating from the nanoparticle in the presence of high protein concentration, or transchelation of the radiometal from the chelator-complex have raised concerns over erroneous interpretation of the imaging results. Moreover, limitations such as specific coordination chemistries, harsh and prolonged reaction conditions, complex purification procedures, and influence on the nanomaterial surface properties and therapeutic loading capacity, have prompted development of intrinsically radiolabeled nanoplatforms.[20]

To overcome the limitations of traditional radiolabeling methods, nanoparticles have been uniquely employed for chelator-free or direct incorporation of the radionuclide into the nanoparticle core. Intrinsic radiolabeling strategies can be classified as follows: (*1*) mixing radioactive and cold precursors during the synthesis of the nanoparticle, (*2*) specific trapping of certain nuclides into the nanoparticles *via* coordination bonding, (*3*) ion-exchange mechanisms, and (*4*) ion bombardment.[20] Incorporation of trace amounts of radioactive precursor during synthesis results in stable formulations, with high radiochemical yields. However, longer labeling times, potential lattice mismatch between the radionuclide and nanoparticle, prolonged exposure to the personnel and generation of excessive radioactive waste; limit the applicability of the process. Post-synthesis radiolabeling has thus, gained wider acceptance. Specific trapping is a more generalized approach, shown to be highly successful for a number of isotopes (^{64}Cu [21], ^{89}Zr [22, 23], ^{72}As [24] and ^{69}Ge [25], *etc.*) and nanoplatforms. Ion exchange methods have also been variously applied to radiolabel lanthanide-doped upconversion nanoparticles with ^{153}Sm for SPECT [26], and ^{18}F [27] and ^{64}Cu [28] for PET. Proton beam activation is another promising strategy, applied till date on Al_2O_3 nanoparticles to produce [^{18}F]-labeled Al_2O_3. [29, 30] The readers are directed to our earlier review for comprehensive details about each technique. [20]

Lastly, selection of the right nanoplatform is of utmost importance. Factors that influence the choice of the nanomaterial include chemical composition, intrinsic functionality, colloidal stability, hydrodynamic size, surface characteristics, ease of surface modification, addition of imaging and therapeutic moieties and ligands for target recognition, *etc.* A plethora of

nanoplatforms have been designed for PET integrated Theranostics (Table 1). In the following sections, we will discuss the state-of-the-art in nuclear nanomedicine, focusing on the recent advances in the evolution of inorganic radiotracers.

4. Radiolabeled Nanomaterials for Cancer Theranostics

4.1. Radioactive Silica Nanoparticles

Silica, “Generally Recognized as Safe” (GRAS) by the Food and Drug Administration (FDA) [31] is among the most biocompatible and well-tolerated inorganic nanomaterials, being endogenous to humans and other animals. The widespread use of silica nanomaterials in multimodal imaging is interesting because unlike other inorganic nanoparticles, these do not possess intrinsic properties to directly serve as contrast or therapeutic agents. However, the well-defined siloxane chemistry for easily tunable size, morphology and porosity, as well as facile surface functionalization, give silica nanomaterials a distinct edge over their counterparts.[32] Their inability to absorb wavelengths in the electromagnetic spectrum and non-interference with the magnetic fields has been utilized in complexing with other functional nanomaterials and drugs to design multifunctional agents (Table 2).[33–35] Moreover, high surface area-to-volume ratio, rigid and stable skeletal network and well-established, scalable synthetic procedures are added advantages, propelling their application as contrast agents in cancer theranostics.

Silica-based ultrasmall (6–7 nm sized) core-shell hybrid nanoparticles (also known as C dots, or Cornell Dots) were approved by the US FDA in 2010 as an investigational new drug (IND), and were reported recently for imaging in patients with metastatic melanoma.[36, 37] Cy5 dye-loaded C dots (<10 nm) were labeled with ^{124}I for PET imaging and conjugated with PEG and cRGDY peptide for detection of integrin-expressing lesions. The tracers were well tolerated, exhibiting good *in vivo* stability, reproducible pharmacokinetic signatures consistent with renal clearance, and preferential accumulation at the target site (Figure 2). However, several synthetic challenges prompted the group to design a more biologically competent, water-based approach for the preparation of <10 nm fluorescent, core-shell nanoparticles (called C’ dots) with different core compositions and enhanced quantum yields (~0.8; nearly approaching the theoretical brightness limit).[38]

Besides the ultrasmall C dots, 20–25 nm sized, dye-incorporated dual-modal silica nanoparticles have also shown promising results for sentinel lymph node imaging and clearance kinetics.[39, 40] Despite these encouraging results, the application of silica nanoparticles in theranostics has remained elusive due to the challenges in encapsulating drugs/therapeutics into the nanoparticles. With their tailored porous structure and high surface area, mesoporous silica nanoparticles (MSNs) show significant advantages over traditional drug nanocarriers, resulting in an exponential rise in their biomedical applications since the first report in 2001.[41, 42] Our group first demonstrated CD105-specific, *in vivo* PET imaging and image-guided doxorubicin delivery with antibody conjugated MSNs in 4T1 breast cancer.[43] Uniform (~ 80 nm) MSNs (synthesized *via* a soft-template method) were conjugated to TRC105 antibody *via* PEG linkers and subsequently functionalized with NOTA for ^{64}Cu chelation. Serial PET scanning demonstrated rapid and persistent accumulation of the nanoconjugates at the tumor site (5.9 ± 0.4 %ID/g at 5 h post-injection

(p.i.)) which was attributed to both EPR effect and TRC105-mediated binding to CD105 (over expressed in tumor vasculature). Enhanced CD105-targeted delivery of doxorubicin was also demonstrated simultaneously, clearly demonstrating the superiority of surface functionalized MSNs in targeted theranostics. The strategy could be tailored to target different biomarkers and tumor models [44], or to develop multimodal imaging agents.[45] Moreover, the facile silica chemistry has been harnessed for radiolabeling with varied isotopes ranging from very short lived ^{18}F ($t_{1/2}$ = 109.8 min)[46] to longer lived ^{89}Zr ($t_{1/2}$ = 72.8 h) [47] *via* simple one-step reactions with appropriate chelators.

Further improvement in the morphology of silica nanoparticles was achieved by designing hollow MSNs (HMSNs) with a large interstitial cavity and a mesoporous shell.[48, 49] HMSNs with low density and high specific area, showed extraordinarily high drug loading capacity [50] and could integrate various functional nanocrystals for multimodality imaging (MR/upconversion/ultrasound) and therapy.[51–54] We recently reported an HMSN based dual modality PET/near-infrared fluorescence (NIRF) imaging agent by conjugating zwitterionic dye, 800ZW and PET tracer ^{64}Cu.[55] As-synthesized HMSNs could load up to 1129.2 mg doxorubicin per gram of HMSN (3–15 times higher than reported MSNs). Enhanced CD105 specific tumor accumulation (~9.9 %ID/g) was observed after conjugation with TRC105, making surface engineered HMSNs a highly attractive drug delivery nanoplatform for future cancer theranostics.

Though chelator-free radiolabeling has been demonstrated with several nanoparticles, most reports suffer from the same specificity issues as traditional chelator-based methods. This problem was recently overcome by the discovery of intrinsic radiolabeling ability of silica nanomaterials. Amorphous dense silica nanoparticles have been shown to serve as general substrates for chelator-free radiolabeling of ^{22}Na [56] and six medically relevant radiometals (^{68}Ga, ^{64}Cu, ^{89}Zr, ^{90}Y, ^{111}In, and ^{177}Lu), with the labeling characteristics depending on the oxophilicity of the radioisotope.[22] Schaffer *et al.* demonstrated that >99 % labeling yields could be obtained for all isotopes at pH = 7.3, 70 °C and incubation times up to 1 h (when specific activity ~100 Ci/μmol), while stability of the binding correlated with hardness of the radioisotope. However, long-term *in vivo* radiostability tests performed by our group demonstrated that while dense silica nanoparticles could chelate ^{89}Zr, such binding was weak with the isotope detached from the nanoparticles *in vivo* and accumulated in the bones (^{89}Zr is a well-known osteophile) within a day of intravenous administration. [23] Systematic studies demonstrated that MSNs could serve as a more reliable platform for radiolabeling oxophilic radiometals with >20-fold higher radiostability than the dense silica nanoparticles, indicating a crucial role of mesochannels in stabilizing ^{89}Zr inside MSNs (Figure 3). This difference in *in vivo* stability profile was rationalized by the presence of mesochannels, which not only protect the guest ^{89}Zr ions from transmetallation by intrinsic protein chelators in the body, but also provide a higher number of surrounding deprotonated silanol groups ($Si\text{-}O^-$) for stronger coordination with the isotope. Although PET imaging is highly sensitive and quantitative for *in vivo* applications, its spatial resolution (mm level) is significantly lower than that of MRI (typically <500 μm). Taking advantage of the easily tailorable chemistry of silica, Burke *et al.* synthesized ^{68}Ga radiolabeled silica coated iron oxide nanorods to combine the high sensitivity of PET with MR contrast.[35] As with ^{89}Zr, ^{68}Ga is a hard Lewis acid that coordinates easily and stably with the Lewis base

donor atoms like oxygen from the silanol groups. PEG modified nanoconjugates were further used for high sensitivity liver imaging. This facile and robust radiolabeling technique holds important implications for nanomedicine. Firstly, it can allow systematic and long-term tracking of nanoparticle biodistribution, thereby providing accurate, real-time information on their *in vivo* fate, biodegradation rates and clearance pathways, potential toxicity, drug delivery, and chemotherapeutic efficacy. Secondly, by simply incorporating certain functional groups, MSNs can directly and stably chelate other radioisotopes, for example, ^{64}Cu and ^{72}As, making them a versatile chelation platform. Lastly, labeling with radiotherapeutic isotopes (like ^{111}In, ^{177}Lu, *etc*.) can open up new possibilities for theranostics with simultaneous radiotherapy and drug delivery.

4.2. Radioactive Carbon Nanoallotropes

Carbon nanomaterials are lower dimensional carbon allotropes that have garnered great attention in the past few decades, since the discovery of fullerenes in 1985,[57] compounded further by the discoveries of carbon nanotubes (CNTs) [58], graphene [59] carbon dots [60, 61] and nanodiamonds.[62] (Figure 4) The nanomaterials range typically between 1 nm-1 μm, and have been employed as optical imaging and therapeutic agents as well as drug nanocarriers in biomedical applications, owing to their unique electronic structure and readily tunable shapes and sizes.[63] The strong absorption in NIR and far NIR (NIR II) windows (750–1000 nm and 1000–1700 nm, respectively), allows deep tissue imaging with high resolution, enhanced contrast and minimized autofluorescence and photobleaching, leading to widespread applications in optical and photoacoustic imaging, photothermal imaging and therapy. [64–68] In addition, CNTs, graphene and carbon dots exhibit strong and unique G-band peaks in the Raman scattering spectrum, which have been harnessed for multiplexed, multicolor Raman imaging, both *in vitro* and *in vivo*.[65, 69, 70] Large surface area and abundance of π electrons has further allowed loading of hydrophobic drugs *via* π-π interactions for efficient delivery in physiological conditions.[71] The unique properties of carbon nanomaterials have been exploited to develop novel multiplexed, multifunctional nanoprobes consisting of biologics, radionuclides, drugs and optical probes, *etc*.

In nuclear medicine, biological properties of CNTs have been explored *in vivo via* PET or SPECT, using radionuclides like ^{125}I[72], ^{111}I[73], ^{99m}Tc[74]. Both single-walled (SWNTs) and multi-walled (MWNTs) nanotubes demonstrated small active molecule-like rapid clearance from systemic blood circulation, effortless transportation through tissues and organs, and rapid renal clearance, with no retention in the RES. However, other biodistribution studies with ^{86}Y-DOTA-SWNT and ^{111}In-DOTA-SWNT reported by McDevitt *et al*.[75] and [^{14}C]-labeled MWNTs, reported by Georgin *et al*.[76, 77] demonstrated contradictory results with major accumulation in the RES and much slower hepatobiliary clearance. Liu *et al.* first demonstrated tumor-targeted PET imaging with ^{64}Cu-DOTA radiolabeled SWNTs, functionalized with phospholipid and PEG to impart longer blood circulation, superior hydrophilicity and reduced RES uptake.[78] Conjugation with cRGDyK peptide conferred integrin $\alpha_v\beta_3$ specific uptake in U87MG glioblastoma xenografts (~13 %ID/g), attributed to the multivalency effect of SWNTs, which was further confirmed by the unique Raman signatures of the nanoprobes. Similarly, antibody [79, 80] and hyaluronic acid [81] functionalized CNTs have been explored for multimodality cancer

theranostics. Furthermore, chelator-free radiolabeling of SWNTs has also been reported, whereby metal halide $Na^{125}I$ was filled in the nanotubes by direct covalent conjugation and capped off to prevent any leakage.[82] In further studies, alpha-emitters like $^{225}Ac^{3+}$ [83] and beta-emitters like $^{64}Cu^{2+}$ [84] along with Gd^{3+} ions were stably loaded into the bores of the ultrashort nanotubes by simple sonication, and employed for radioimmunotherapy and PET/MR imaging, respectively. The strategy potentially protects the encapsulated radioisotopes from transmetallation, thereby preventing any leakage and consequent off-target toxicity *in vivo*. However, it is noteworthy that in both the studies, the radiolabeled CNTs accumulated rapidly in the lungs, possibly due to aggregation, which may influence the actual *in vivo* radiostability since the nanoparticles are removed quickly from the circulation. Further studies are warranted to establish the legibility and superiority of this strategy, over traditional chelation methods and further evaluate its suitability for longer-circulating biologically active nanotubes for *in vivo* imaging.

Besides CNTs, graphene is the other nanocarbon allotrope that has gained widespread acceptance in the biomedical community. Single-layered graphene shows ultra-high surface area with every atom exposed on the surface, thereby providing immense opportunities for bioconjugation, drug and gene delivery. The unique electronic and optical properties have been harnessed for phototherapy [85], while the surface itself can be used for growth of various inorganic materials for multimodality imaging and theranostics. [86, 87] While Yang *et al.* [68] first studied the *in vivo* biodistribution and tumor ablation ability of PEG-modified, Cy7 dye labeled nanographene sheets in U87MG tumor-bearing mice, the inherent limitations of optical imaging, mainly autofluorescence and tissue depth limitations, prompted the need of radionuclide imaging for a more accurate assessment. Our lab first reported PET imaging of ^{64}Cu-NOTA conjugated, PEGylated graphene oxide (GO), specifically directed to the tumor neovasculature, through targeting the CD105 receptor, as evidenced by the rapid, persistent and CD105 specific uptake in 4T1 metastatic breast tumors.[88] Graphene oxide nanosheets have been widely employed for developing passively [89] and actively targeted agents [90–92], radiotracers for isotopes like ^{66}Ga[93], ^{125}I[94] ^{111}In[95], and theranostic agents [85, 92, 96, 97]. Of note, however, while intrinsic radiolabeling techniques have been applied to CNTs, graphene is yet to benefit from the merits of these novel methodologies.

Despite being around for decades, long-term toxicity concerns have severely impeded the clinical translation of CNTs and graphene; prompting the introduction of other lower dimensional nanocarbons into the biomedical arena. PET imaging with carbon dots [98], nanodiamonds [99] and fullerenes [100] is an emerging field, with initial studies dedicated solely to the assessment of their *in vivo* biodistribution. For example, ^{64}Cu-DOTA conjugated fluorescent carbon dots were recently synthesized and their *in vivo* fate was analyzed, following injection *via* three different routes, *i.e.* intravenous (i.v.), intramuscular (i.m.) and subcutaneous (s.c.). Although low RES uptake was observed (<1 %ID/g) within 24 h p.i. with renal clearance in all the groups, the rate of clearance from the blood followed the order: i.v. > i.m. > s.c. [98] It is noteworthy that the other ultrasmall carbon nanoallotropes also demonstrate greatly reduced RES accumulation and rapid clearance predominantly through the renal pathway, potentially addressing the toxicity concerns posed by the use of carbon nanomaterials. However, the rapid clearance compromises on the

enhanced tumor contrast, characteristic of graphitic carbon tracers (Figure 4). Further optimization of *in vivo* pharmacokinetics and tumor homing patterns of these emerging members of the nanocarbon family, as well as their application as multimodality and multiplexing agents, is therefore warranted. Given that one of the major hurdles in the clinical translation of traditional carbon nanomaterials is their substantial and prolonged RES retention, carbon dots, nanodiamonds and fullerenes have much to offer.

4.3. Radioactive Fluorescent Nanomaterials

Fluorescence-based imaging methods have attracted great attention in the last two decades because they are sensitive, selective, rich in contrast, convenient, versatile, non-destructive, widely available and cheap.[101] Compared to the traditional organic dyes, which suffer from short fluorescence lifetimes (1–10 ns), inorganic nanoparticles like quantum dots and upconversion nanophosphors (UCNPs), with longer life-times (typically few hundred nanoseconds), improved optical characteristics and multiplexing ability, are better candidates for in vivo optical imaging. For a more comprehensive review of the current state-of-the-art in fluorescence imaging with nanomaterials, readers are directed to these excellent articles.[101, 102] Despite its advantages, optical imaging suffers from limited tissue penetration, autofluorescence and qualitative nature. The combination of fluorescence- and radionuclide-based imaging offers synergistic advantages over each individual modality. In the following sections, we will discuss dual-modality optical/PET imaging with two of the most frequently employed fluorescent agents; quantum dots and UCNPs.

4.3.1. Quantum Dots—Quantum dots (QDs) are inorganic fluorophores (<10 nm) with excellent light-emitting properties that can overcome many limitations of traditional fluorophores. Due to their small size (2–10 nm), QDs display unique properties unavailable in either bulk material or individual atoms, such as size- and composition- tunable emission in a narrow, symmetric energy band, large Stokes' shift (>200 nm), superior brightness and long fluorescence lifetimes, as well as large absorption coefficients across a wide spectrum, stemming from the quantum confinement effects.[103, 104] In addition, resistance to photobleaching and chemical degradation further simplifies the storage and handling requirements.[105] Traditionally, QDs are nearly spherical inorganic semiconductor crystals that consist of a core and shell comprising of elements from heavy metal-containing groups II-IV, IV-VI, or III-V.[106] The core is typically made of cadmium selenide (CdSe) with a ZnS shell. There are many types of QDs commercially available. Some other examples of QD cores include CdTe, PbSe, GaAs, GaN, and InP [107], the quantum yields for which can be drastically enhanced (~90%) by coating with a shell of high-energy bandgap material. For more information about the various types of QDs and their applications, readers are directed to these references.[107–110] As with other nanomaterials, QDs provide a multifunctional nanoplatform for multimodality imaging and therapy, especially suitable for synergistic optical/PET imaging which combines the sensitivity, quantification and limitless tissue penetration of PET with high resolution and specificity of optical methods.[104]

Cai *et al.* reported dual-functional QD nanoprobes for quantitative assessment of *in vivo* pharmacokinetics and tumor-targeting efficacy of QDs using both PET and NIRF imaging.[111] RGD peptide-bearing, ^{64}Cu-labeled QD705 achieved greater tumor contrast in

U87MG xenografts at a fraction of concentration than that needed for *in vivo* NIRF imaging, thereby significantly reducing potential toxicity. Several other studies since then, have explored the use of directly/indirectly radiolabeled QDs for tumor-targeted imaging. [112–117] However, poor long-term radiostability *in vivo* has raised concerns. For example, in several studies, while at earlier time-points the PET and NIRF imaging data were in good agreement, substantial differences could be observed at later time-points, possibly attributed to the detachment of the isotope.[111, 113] Therefore, incorporation of the radionuclide in the QD core has been proposed to eliminate the concerns regarding *in vivo* stability of the radiolabel relative to the QDs, since it is well documented that QDs do not undergo significant degradation unless subjected to very harsh conditions.[118]

Intrinsically radiolabeled QDs were first reported for SPECT/CT imaging where, ^{125m}Tc ($t_{1/2}$ = 58 d) was incorporated into tumor-targeted Cd^{125m}Te/ZnS QDs during the synthetic process.[119, 120] Another study reported the incorporation of ^{109}Cd ($t_{1/2}$ = 464 d) into zwitterionic radioactive-QDs for reliable biodistribution studies *via* gamma counting.[121] While the studies reported high incorporation efficiencies and radiostability, sub-optimal radionuclide characteristics such as long half-lives and low specific activities warrant the use of clinically relevant PET and SPECT isotopes. Sun *et al.* first synthesized ^{64}Cu-doped CdSe/ZnS QDs *via* a cation-exchange reaction, with nearly 100% radiolabeling yield and high radiostability (in bovine serum and mouse blood over 48 h).[28] Incorporated ^{64}Cu not only accurately reflected the *in vivo* biodistribution, but also allowed for efficient Cerenkov resonance energy transfer (CRET) imaging in U87MG glioblastomas. ^{64}Cu-doped QDs exhibited rapid and persistent uptake in the U87MG tumor; ~5% ID/g at 1 h time point, which reached 12.7% ID/g at 17 h p.i. (Figure 5). Currently, CRET is a hot topic in the field of molecular imaging as these imaging agents do not require external excitation sources; thus, CRET overcomes a key limitation of fluorescence imaging. Several researchers have successfully employed radiolabeled QDs for Cerenkov luminescence imaging.[122–125]

4.3.2. Rare-Earth Upconversion Nanophosphors—Rare-earth UCNPs have recently emerged as promising candidates as a new generation of multifunctional and multimodality nanoplatform for personalized theranostics. Upconversion luminescence (UCL) refers to a unique non-linear process whereby multiple low energy photons (near-infrared) are sequentially absorbed or undergo energy transfers to emit higher energy (visible to ultraviolet) light. [126, 127] The basic structure of UCNPs consists of an inorganic host matrix (fluorides, oxides, heavy halides etc.), a sensitizer (to enhance UCL efficiency; Yb^{3+}) and an emitter (Er^{3+}, Tm^{3+} and Ho^{3+} dopant ions). Lanthanide doping into the host material confers UCNPs with several advantages over conventional luminescence probes; namely sharp emission bandwidths, large anti-Stokes shifts, excellent photostability, non-blinking, minimal autofluorescence, and deeper tissue penetration.[126, 128] Structure, fabrication, characteristics and optical imaging applications of UCNPs have recently been reviewed in excellent articles.[126–131] Owing to the well-established synthetic procedures and facile surface chemistries, UCNPs are increasingly being employed for diverse applications such as cell tracking [132], small animal imaging [130], drug delivery [133], photothermal [134], photodynamic [133] and combination therapies. [135, 136]

Multiple functions embedded in a single nanoparticle can play a crucial role in precise disease diagnosis and thus, the use of functionalized UCNPs as multimodal contrast agents is under active exploration.[137] Simple variations in dopant atoms or lattice composition can endow UCNPs with MR, PET, SPECT and CT imaging capabilities, in addition to their intrinsic UCL property.[129] Interestingly, chelator-based PET imaging with UCNPs has been rarely reported, with one study reporting DOTA chelated ^{68}Ga labeled UCNPs for integrin $\alpha_v\beta_3$ targeted PET imaging in M21 tumor models.[138] In a more recent study, bimodal *in vivo* imaging was employed to demonstrate hepatobiliary excretion of micelle-encapsulated UCNPs *via* PET and upconversion luminescence imaging.[139] ^{64}Cu-NOTA-UCNPs displayed high radiochemical purity (~99%) and reasonable serum stability (100 % upto 4 h and ~75% after 24 h). The multiplexing capabilities of UCNPs were very ably demonstrated in a recent exciting study by Rieffel *et.al* who reported a hexamodal porphyrin-phospholipid-coated UCNP (PoP-UCNP) system, where the exquisite affinity of copper for porphyrins was used for post-labeling of UCNPs with ^{64}Cu by simple incubation (>80% labeling yield).[140] PEGylated PoP-UCNPs (~74 nm) were further employed for *in vivo* lymphatic mapping (Figure 6). With just two active imaging components, fluorescence, NIR-to-NIR UCL, PET, CT, Cerenkov luminescence, and photoacoustic tomography (PAT) could be performed, exemplifying the feasibility of simple yet higher order multimodality imaging agents. In another noteworthy study, integrin $\alpha_v\beta_3$ targeted, Er^{3+}/Yb^{3+} co-doped $NaGdF_4$ UCNPs were reported. UCNPs were radiolabeled with ^{124}I ($t_{1/2}$ = 4.2 days) using a tyrosine residue of $(cRGDyk)_2$ ligand, thereby creating a clinically relevant trimodal (UCL/MR/PET) agents with synergistically acting imaging capabilities.[141]

Research on intrinsically radiolabeled UCNPs has also been on the rise. For example, SPECT imaging has been achieved by introducing Samarium-153 (^{153}Sm; $t_{1/2}$ = 46.3 h) ions into the UCNP lattice, either by co-doping during hydrothermal synthesis [142–145] or *via* cation-exchange based post-labeling method.[26] Notably, chelator-free radiolabeling if UCNPs with PET isotopes has been seldom explored. Although, the incorporation of ^{18}F into the UCNP matrix *via* specific trapping or cation assisted ligand exchange reactions has been well documented [27, 146–148], the relatively short half-life of ^{18}F ($t_{1/2}$: 109.7 min) and limited applicability to selected radioisotope: host combinations, warrants development of alternative labeling procedures to fully utilize the vast repertoire of more suitable isotopes.

While inorganic optical imaging agents have been around for more than two decades, several issues have hampered their prospects for clinical translation. Structural complexities, heavy metal compositions, potential toxicity, prolonged *in vivo* residence, suboptimal stability and clearance kinetics as well as in effective tumor-targeting, have elicited concerns. For instance, newer QDs have been designed from silicon and certain polymers, in an effort to minimize potential toxicities and make them more biocompatible,[149–151] Similarly, efforts are also being concentrated towards developing renal clearable [15] and biodegradable quantum dots [152] and ultrasmall UCNPs [153]. Further challenges, in terms of their synthesis, surface functionalization, stability, *in vivo* pharmacokinetics and tumor-targeted imaging remain to be conquered. In this regard, synthesizing sub-10 nm UCNPs may not only improve their renal clearance profile and minimize toxicity, but may also aid in enhanced tumor-cell targeting.[154].In addition, cancer theranostics, whereby therapeutic

components are combined with the multimodal imaging capacity of QDs and UCNPs into a single vector, also presents a relatively lesser explored, yet promising avenue for research. Further multidisciplinary efforts are required to optimize these nanoplatforms to fully realize their potential in cancer prevention, diagnosis, therapy, patient-stratification and management.

4.4. Radioactive Gold Nanomaterials

Owing to their unique physicochemical properties, varied and tailorable shapes, sizes and chemical compositions, gold nanostructures make excellent candidates for molecular imaging and, potentially, therapy of various diseases, including cancer [155, 156], cardiovascular disease [157–159], viral infections [160–162], and others.[163, 164] Gold nanoparticles (AuNPs) display excellent biocompatibility as gold is relatively inert in biological environments.[165] They also possess unique plasmonic properties that allow researchers to track their biodistribution *in vivo*.[166] The unique surface plasmon resonance peaks of gold nanostructures can be easily tuned between visible and NIR windows by simply changing the shape and size of AuNPs, which has been variously harnessed for FL, PA and Raman imaging, as well as for photothermal therapy (PTT).[167–171] Furthermore, AuNPs can be easily functionalized with active or passive targeting entities through interactions between gold and thiol-containing compounds.[172, 173] Lastly, many gold-based nanoplatforms have been shown to effectively load large drug payloads with optimal release kinetics for targeted delivery to diseased tissues. [174–177]

The biggest advantage of AuNPs in imaging lies in their multiplexing ability. The inherent optical properties and high X-ray absorption coefficient allows their use as multimodal contrast agents, with widespread applications in optical, MR, CT and radionuclide imaging. [178] For example, sharply branched gold nanostars, with tip-enhanced plasmonic properties have been used in multimodality imaging and phototherapy.[172, 179–182] Interestingly, the shape of gold nanoparticles can significantly impact their biodistribution *in vivo*, influencing the rate of clearance by the RES organs [183, 184], rate of endocytosis [185, 186], and transport of the nanoparticles through the blood.[187, 188] As such, SPECT and PET imaging have emerged as an important tool for tracking the *in vivo* pharmacokinetics of AuNPs. AuNPs and nanorods, radiolabeled with ^{99m}Tc[189], ^{125}I and ^{111}In[190, 191] have been utilized for targeted SPECT imaging. Xie *et al.* first reported the biodistribution of Au nanoshell-coated silica cores, radiolabeled with ^{64}Cu *via* bifunctional chelating agent DOTA, in head and neck squamous cell carcinoma (HNSCC) xenograft-bearing rats.[192] In addition to nanoshells [193, 194], chelator-based PET studies have extensively been carried out for other AuNP morphologies like nanospheres [195–198], hollow nanospheres[199, 200], nanostars[180], nanocages[201], nanorods[202], nanotripods[203], nanodumbells [204], and ultrasmall nanoparticles [205, 206] (Figure 7a–f). In these studies, PET was successfully used to assess the biodistribution and tumor accumulation of radiolabeled nanoplatforms. For example, Cheng *et al.* reported the synthesis of novel, anisotropic, branched Au-tripods (size <20 nm), functionalized with cRGD peptide for targeting U87MG xenografts in mice *via* dual modal PAT and PET.[203] At 24 h post-injection, PET imaging revealed ~7.9 %ID/g of RGD-Au-tripods in the U87MG tumors, about 3 times higher than the blocking group. In addition, the authors noted that there were no signs of acute or

systemic toxicity. However, toxicity normally does not occur until tissues have been exposed to the gold nanoparticles for 7–30 days, warranting further long-term studies. [207]

In an effort to improve the radiostability, scientists have intrinsically radiolabeled AuNPs, with the earlier studies incorporating Au-198 (β_{max}=0.96 MeV; $t_{1/2}$=2.7 d) and Au-199 (β_{max}=0.46 MeV; $t_{1/2}$=3.14 d) for radiotherapy [208, 209], SPECT [210] and radioluminescence imaging.[211, 212] In 2014, Zhao *et al.* reported the use of ^{64}Cu-alloyed AuNPs, where radioactive $^{64}CuCl_2$ precursor was mixed with 'cold' Au precursors during the synthesis.[213, 214] Similarly, Sun *et al.* demonstrated post-synthetic chelator-free ^{64}Cu radiolabeling of different Au morphologies by simple hydrazine-mediated reduction of the $^{64}CuCl_2$ precursor on the surface of the PEGylated nanoparticles.[21] While effective as contrast agents, AuNPs demonstrated high liver and spleen uptake, which is a common limitation of most intravenously administered nanoparticles. To overcome these limitations, Zhao *et al.* synthesized ultrasmall ^{64}Cu-labeled gold nanoclusters for PET imaging of prostate cancer in a mouse model.[215] The 5 nm sized nanoparticles were PEGylated with 5-kDa PEG and the biodistribution studies revealed significant renal and hepatobiliary excretion, thus showing that some liver and spleen uptake can be avoided by modifying the clearance mechanism of the nanoparticles. It is well known that nanoparticle size can significantly impact its biodistribution *in vivo*. Smaller, renal clearable nanoparticles are better suited for clinical translation as they are not restricted by toxicity concerns. The kinetics of renal clearable nanoparticles were further analyzed by dynamic PET imaging of ~3 nm sized ^{64}Cu-NOTA-Au-GSH.[206] When compared to previous studies[216], ^{64}Cu-NOTA-Au-GSH demonstrated rapid renal clearance (>75%ID at 24 h post-injection) and drastically reduced hepatic uptake, with an elimination half-life (< 6 min, over 130-times shorter than previously reported for similar nanoparticles), demonstrating potential as imaging agents in models of acute renal failure and other renal diseases (Figure 7g–i). As discussed in this section, radioactive gold nanoparticles make excellent theranostic agents when they are effectively synthesized. Further in-depth pharmacokinetic studies are needed for successful clinical translation in the future.

4.5. Radioactive Magnetic Nanoprobes

Non-invasive MRI is characterized by high spatial resolution (~sub-millimeter level) and exquisite soft tissue contrast.[8] However, the inherent low sensitivity of MRI has spurred rapid development of exogenous contrast agents.[217, 218] Integrated PET/MR imaging forms a powerful modality, combining excellent soft tissue contrast and functional imaging parameters provided by MR with high sensitivity and quantification of radiotracer metabolism provided by PET.[219, 220] Interestingly, even though the idea of simultaneous PET/MR imaging has been around since the 1990s, virtually no dual modality contrast agents were reported until a few years back, for the lack of suitable equipment.[221] With rapid strides in technology, prototype PET/MRI systems have been successfully conceived for small-animal imaging, accelerating the research for novel bimodal magnetic radiotracers. [222, 223] Synchronous PET/MR imaging has the potential to become the imaging modality of choice for various clinical applications such as neurological studies, certain types of cancer, stroke, and the emerging field of stem cell therapy, warranting the development of hybrid PET/MR probes.[8] Depending on the constituents of the contrast agents, magnetic

nanoparticles can be categorized into (i) superparamagnetic iron oxide nanoparticles (SPIONs) based T2 contrast agents, and (ii) paramagnetic gadolinium (Gd) or manganese (Mn) based T1 contrast agents. Readers are directed to these excellent reviews for a more comprehensive understanding of the fabrication, surface chemistry and biological applications of magnetic nanoparticles.[224–227]

In recent years, SPIONs have emerged as one of the most promising contrast agents in MRI for disease diagnosis and treatment monitoring. Phenomenal advances have been made in engineering iron oxide based magnetic contrast agents in terms of composition, structure, biocompatibility, relaxivity and contrast effects [217, 228, 229] and several SPION formulations have been approved in the clinic, such as Ferridex I.V.® for liver and spleen imaging, Ferumoxytol® for iron replacement therapy, and Combidex® for imaging lymph node metastases.[230]

SPIONs have been labeled with multiple radioisotopes for both SPECT (^{99m}Tc [231, 232], ^{125}I [233], ^{111}I [234, 235], ^{125}I [236] and ^{131}I [237, 238]) and PET.[239] Traditional approach involving chelating agents such as DOTA [240–243], NOTA [204, 244, 245], DTPA [246] and bis(dithiocarbamatebisphosphonate) (DTCPB) [247, 248] for ^{64}Cu and ^{68}Ga, and DFO for ^{89}Zr [249] has been reported in an array of differently designed and surface-functionalized SPIONs. For example, Thorek and coworkers reported a simple ^{89}Zr-labeled version of clinically relevant ferumoxytol with excellent toxicity and clearance profile, for high resolution investigation of lymphatic drainage in murine cancer models. [249] The nanoformulation not only allowed for clear preoperative mapping for nodal resection, but also provided non-invasive intra-operative guidance for tumor staging and therapy planning. Besides radiometals, traditional radioisotopes like ^{18}F[250], ^{11}C[251] and ^{124}I[252] have also been variously used for dual PET/MR imaging *in vivo*.

Development of new radioisotopes for PET imaging and lack of chelators thereof has prompted active research in the development of intrinsically radiolabeled SPIONs. Owing to their versatile chemistry, SPIONs have served as perfect hosts for some isotopes, which were difficult to label *via* traditional chelator-based routes.[253] For example, our group recently demonstrated intrinsic labeling of radioarsenic (*As^{III} and *As^{V}, *=71, 72, 74, 76) and germanium-69 (^{69}Ge; $t_{½}$ = 39.05 h, 21% β^+, E_{max} = 1205 keV) at the surface of SPIONs. [24, 25] (Figure 8) Rapid and specific labeling with high yields could be achieved simply by mixing water soluble poly(acrylic acid) (PAA)-modified SPIONs with these isotopes. PEGylated radiolabeled SPIONs were further used for *in vivo* PET/MR imaging and sentinel lymph node mapping. In addition, conventional radiometals, such as ^{64}Cu[254] and ^{68}Ga [255], have also been incorporated into SPIONs to develop novel multimodal tracers For example, heat induced ^{89}Zr binding on ultrasmall magnetite cores (120 °C, pH 8) resulted in a radiochemical yield of ~93% and high stability as determined by *in vivo* PET/CT and biodistribution studies.[256] ^{64}Cu and ^{111}In radiometals could be similarly labeled indicating that tight metal ion binding to the magnetite crystal surface could likely be due to interaction between the positively charged metal ions and the anionic oxide surface layer. [256] The strategy was also applied to feraheme nanoparticles for monocyte tracking. [253] Furthermore, the technique can potentially be extended to other metal/metal oxide-based nanoparticles to develop novel, clinically translatable, multimodality PET/MR radiotracers.

One of the most frequently used contrast agents in clinics (Gd^{3+} chelates) comprises of paramagnetic complexes (usually Gd^{3+} and Mn^{2+}) that shorten the longitudinal (T1) relaxation time of water, thus increasing the signal intensity of T1 weighted MR images.[257, 258] To develop more efficient agents with larger number of magnetic centers, Gd/Mn based nanomaterials are being steadily developed.[225, 259] However, the progress of dual modal paramagnetic radiotracers is still slow paced.[260–262] Huang *et al.* first reported the synthesis of water soluble human serum albumin (HSA)-coated MnO nanoparticles (MONPs), which were subsequently used for dual modality PET/MR imaging in U87MG murine xenografts after ^{64}Cu-DOTA coupling.[260] R_1 relaxivity of HSA-MONPs was evaluated to be 1.97 $mM^{-1}s^{-1}$ which is close but inferior to the clinical standard, Magnevist (5 $mM^{-1}s^{-1}$). In another noteworthy study, radioactive fluorimagnetic $GdVO_4$:Eu^{3+} tetragonal ultrathin nanosheets were developed and evaluated for PET, fluorescence and T1-weighted MR imaging in PC-3 prostate tumor bearing mice.[262] The nanoconjugates were labeled with ^{64}Cu *via* DOTA chelation and integrin $\alpha_2\beta_1$ targeting was achieved *via* Asp-Gly-Ala (DGEA) peptide conjugation. The R_1 value was estimated to be 33.25 mM^{-1} s^{-1}, approximately 7 times higher than the commercial T_1-enhanced MRI agents.

Recent efforts to integrate multiple modalities have led to nanosystems with not only augmented diagnostic capabilities, but also simultaneous drug delivery and therapeutic functionalities. Important capabilities of magnetic nanoparticles for therapy are the external control of magnetic heat generation and magnetic attractive forces for enhanced transportation and targeted movement of nanoparticle-conjugated therapeutic moieties.[263] While theranostic applications of parmagnetic nanomaterials are yet to be explored, reports using SPIONs span over a wide range and include drug delivery [227, 264, 265], gene therapy [266], immunotherapy [267], hyperthermia [268–271] and photodynamic therapy (upon complexation with photosensitizers) [272].

4.6. Other Radioactive Nanomaterials

Search for novel and effective agents with improved imaging and therapeutic outcomes is the primary fuel for innovations in molecular theranostics. In addition to the already established arsenal of nanoradiotracers, numerous other nanomaterials have been engineered and explored for use in cancer theranostics in the past few years. For instance, chalcogenides, especially copper sulfide nanoparticles (CuS NPs) have gained significant attention from the research community as photothermal contrast agents and have been employed for several biomedical applications including PAT [273–275], PTT [276–278], and drug delivery [279]. Similar to many other nanoplatforms discussed in this article, CuS nanoparticles may be synthesized in different shapes and sizes; nanospheres, nanocages, nanoflowers, nanoplates, nanotubes, nanorods, and nanowires[280]. Zhou *et al.* first developed radiolabeled CuS nanoparticles, where ^{64}Cu was integrated into the CuS matrix, for combined PET imaging and photothermal ablation of tumors.[281] The strategy was extended to develop CuS NPs for tumor-targeted PET imaging-guided photothermal therapy [17], combined radio- and photothermal therapies [282, 283], and ultrasmall CuS nanodots.[284] While addition of radioactive precursor during synthesis ensures high incorporation efficiency, the cumbersome chemistry and handling procedures impede clinical translation.[20] Riedinger *et al.* recently proposed a post-synthetic mechanism for incorporation

of ^{64}Cu(I) radionuclides in covellite nanocrystals (CuS NCs) by reduction with ascorbic acid. High radiochemical yield (~50 %) and radiochemical purity (~99 %) could be obtained by simply mixing the NCs with $^{64}CuCl_2$ and vitamin C at room temperature.[285] In another report, the affinity of ^{64}Cu for dichalcogenides was exploited by Liu *et al.* to develop a tetramodal (PET/MR/PAT/PTT) theranostic agent based on self-assembled MoS_2 nanosheet and iron oxide nanocomposites.[286] Strong PAT signals and obvious darkening effects in T_2 weighted MR images indicated prominent, time dependent passive tumor retention of double-PEGylated nanoconstructs, further corroborated by quantitative PET data (~6%ID/g accumulation in tumors). Complete tumor resection was seen within 14 days upon irradiation with 808 nm laser (0.78 W cm^{-2}, 5 min) 8 h after i.v. injection of MoS_2-IO-(d)PEG. Similarly, $FeSe_2$-decorated Bi_2Se_3 nanosheets were developed by the same group for tetramodal imaging (PET/CT/PAT/MR) and integrated photothermal-radiation therapy.[287] Though preliminary, these studies highlight the promising potential of transitional metal dichalcogenides for multimodal image-guided cancer therapy. In addition, other nanomaterials; copper nanoparticles and nanoclusters [288, 289], oxides of titanium [290], zinc [291], aluminum [29, 30], cerium [292], layered double hydroxides [293], and oxysulfides [294] have also shown promising results as multifunctional theranostic radiotracers (Figure 9a–f).

Among the organic nanomaterials, lipid-based nanoparticles, micelles, dendrimers, and polymers are the traditional choices and have been best characterized as PET imaging probes.[295] Porphysomes are a new class of organic, biodegradable nanovesicles, composed of porphyrin and lipid bilayers. The porphyrin component allows direct loading of ^{64}Cu into the tetrapyrrole ring without compromising their intrinsic photothermal properties and *in vivo* pharmacokinetics.[296, 297] [^{64}Cu]porphysomes demonstrated good *in vivo* radiostability and selective uptake in orthotopic prostate tumor models. Other porphyrin-based systems have since been utilized for development of multifunctional nanoprobes for a variety of applications.[140, 298–301] Recently, there is an upward trend of employing nanoparticles with intrinsic biological functionalities for theranostic applications.[302, 303] The biomimetic nanoparticles are biocompatible, biodegradable and most importantly, overcome the precursor toxicity issues that plague the clinical translation of current organic and inorganic nanomaterials. One very interesting example is melanin nanoparticles (MNPs) with intrinsic photoacoustic property and natural affinity for metals ($^{64}Cu^{2+}$ and Fe^{3+}), that could be harnessed for multiple imaging modalities like PET, MR, PAT, photothermal imaging and therapy *via* PTT, all combined into one nanoplatform.[304, 305] Another notable example of biomimicry applied for cancer theranostics is self-assembled ferritin nanocages with inherent propensity to bind metal ions for PET/MR imaging and load photosensitizers, optical dyes and other therapeutic molecules to develop a multifunctional nanoplatform.[306–308] In a recent study, ferritin nanocages were also utilized as templates for controlled synthesis of ultrasmall [^{64}Cu]CuS nanoparticles for PA/PET-directed photothermal therapy.[309] Engineering of biomimetic nanomaterials is an emerging field that holds immense potential for combating several issues presented by the use of synthetic nanomaterials. While bioinspired systems have shown promising outcomes for a variety of biomedical applications, such approaches remain untapped in the field of nuclear nanomedicine. Systems like membrane-coated nanomaterials, tumor cell and

macrophage mimetics, viral vectors and others, have the potential to revolutionize the current state of cancer theranostics, if utilized properly. On the flip side, contemporary biomimetic nanotechnologies lack the exquisite precision and controllability in terms of synthesis, functionalization and characterization that is afforded by inorganic nanoparticles, and which must be addressed before any clinical applications can be envisaged.

5. Conclusion and Future Perspectives

Radiation oncology has emerged as a frontrunner in precision medicine and personalized treatment planning. Integration of nanotechnology into the former promises to bring a paradigm shift in the traditional cancer imaging and therapy regimes. Compared to the currently used biological radiotracers, nanomaterials represent an exciting class of novel molecular probes which can be equipped with various imaging labels, targeting ligands and therapeutic moieties, all on the same vehicle. In this review we presented studies exemplifying our current prowess in developing radiolabeled nanoprobes, and tailoring their structural, physicochemical and surface properties to achieve desired *in vivo* pharmacokinetics and improved imaging and therapeutic outcomes. However, despite its immense initial promise and enormous investment (of capital and resources) over the last decade, nanomedicine has been conspicuous by its absence in the clinic.

With the growing importance of personalized medicine and need for translational research, there is an urgent need to evaluate nanoparticle-induced long-term toxicities as well as effects on reproductive and fetal health. The quantitative nature, limitless tissue penetration and sensitivity of PET can afford excellent means for long-term tracking of radiolabeled nanoparticles in living subjects. For instance, using ^{64}Cu-DOTA labeled MWNTs, Huang *et al.* demonstrated that CNTs might induce genetic background-dependent toxic effects on the normal development of the embryo.[310] Larger-sized MWNTs could move across the blood-placenta barrier, restricted fetal development, and induced brain deformity, while SWNTs and smaller MWNTs showed reduced fetotoxicity. This is an excellent example of the importance of robust risk-assessment of potential toxic responses, particularly long-term toxic effects, and individual-dependent toxic responses, for all nanoplatforms before they can be tested in human subjects to image and treat diseases.

Besides toxicity, three key issues require immediate attention; development of targeted nanoparticles with enhanced selectivity to achieve optimal efficacy, improved *in vivo* pharmacokinetics with minimal accumulation in the RES organs like liver and spleen, and most importantly, complete clearance from the body within a reasonable time. More efforts are required to improve nanoparticle delivery both to and within the tumor. Development of actively targeted nanoparticles, especially for quantification of low expression biomarkers could assist in early disease detection and prevention. Careful selection of the target as well as the targeting ligands (*e.g.* antibody, peptide, small protein) is necessary for achieving optimal specific binding, and must be determined based on the nanoparticle shape, size, charge, surface properties *etc.* Detailed studies must be carried out to understand long-term interactions of the nanoparticles with the tumor and especially the major organs of accumulation such as the liver and spleen. Evasion of the mononuclear phagocyte system (MPS) can be achieved by designing ultrasmall globular renally clearable nanoparticles, as

discussed before. While such nanoparticles promise better imaging characteristics, the short circulation time, rapid clearance and attenuated tumor accumulation might hinder their therapeutic potential. Biodegradable nanoparticles with chemically unstable structures may prove more useful in this regard. We recently reported a biodegradable silica platform, tuned to carry large payloads of both small and large molecular drugs, circulate longer in the blood, actively target the tumor vasculature for maximum therapeutic effect, and degrade and clear from the body after serving its purpose.[311] However, such results are preliminary; complete and in-depth evaluation of the nanoparticle properties, dosages required to achieve the desired effects, systemic accumulation, tissue and organ distributions, excretion profiles, and long-term effects of nanoparticle administration, is urgently needed for nanomedicine to make any appreciable mark in the field. In addition, considering the important role that PET can play in profiling the biological fate of nanomaterials, development of facile, robust, stable and personnel-friendly radiochemistry is a prerequisite.

Despite the lackluster performance of nanomaterials in clinical translation, nanomedicine continues to be a fascinating area of research with distinct advantages to healthcare, if properly harnessed. Efforts must be made to tailor the medical applications to nanoparticle properties. For example, nanoparticles exhibiting enhanced RES sequestration can be harnessed for immunotherapy and vaccine development. Phototherapeutic nanomaterials can be used to treat solid tumors, where the resulting hyperthermia can enable deeper nanoparticle/drug extravasation into the tumor recesses. Similarly, magnetic nanoparticles can be employed for magnetic field-guided targeted delivery to disease site, to achieve superior control over nanoparticle transport *in vivo* and enhanced therapeutic indices. Deeper and more rigorous examination of physicochemical and biological properties of the existing repertoire of nanomaterials needs to replace or at least progress in tandem with the current trend of “proof-of-concept” studies. The possibilities are endless, if the scientific community is willing to overhaul the current approach to nanomedicine with a single focus on translation. Concerted multidisciplinary efforts, from scientists, clinicians, funding and regulatory authorities, manufacturing agencies *etc*. may help realize the true potential of nanotheranostics in early-stage disease detection, treatment efficacy, monitoring of disease progression, regression and recurrence in the future.

Acknowledgments

This work is supported, in part, by the University of Wisconsin- Madison, the National Institutes of Health (NIBIB/NCI 1R01CA169365, P30CA014520, and T32CA009206) and the American Cancer Society (125246-RSG-13-099-01-CCE).

REFERENCES

1. Weissleder R. Molecular imaging in cancer. Science (New York, N.Y.). 2006; 312:1168–1171.
2. Weissleder R, Mahmood U. Molecular imaging. Radiology. 2001; 219:316–333. [PubMed: 11323453]
3. James ML, Gambhir SS. A molecular imaging primer: modalities, imaging agents, and applications. Physiol Rev. 2012; 92:897–965. [PubMed: 22535898]
4. Cai W, Chen X. Nanoplatforms for targeted molecular imaging in living subjects. Small. 2007; 3:1840–1854. [PubMed: 17943716]

5. Hong H, Chen F, Zhang Y, Cai W. New radiotracers for imaging of vascular targets in angiogenesis-related diseases. Adv Drug Deliv Rev. 2014; 76:2–20. [PubMed: 25086372]
6. Phelps ME, Hoffman EJ, Mullani NA, Ter-Pogossian MM. Application of annihilation coincidence detection to transaxial reconstruction tomography. J Nucl Med. 1975; 16:210–224. [PubMed: 1113170]
7. Gambhir SS. Molecular imaging of cancer with positron emission tomography. Nat Rev Cancer. 2002; 2:683–693. [PubMed: 12209157]
8. Hong H, Zhang Y, Sun J, Cai W. Molecular imaging and therapy of cancer with radiolabeled nanoparticles. Nano Today. 2009; 4:399–413. [PubMed: 20161038]
9. Jokerst JV, Gambhir SS. Molecular imaging with theranostic nanoparticles. Acc Chem Res. 2011; 44:1050–1060. [PubMed: 21919457]
10. El-Sayed IH. Nanotechnology in head and neck cancer: the race is on. Curr Oncol Rep. 2010; 12:121–128. [PubMed: 20425597]
11. [Accessed: April 30, 2016] https://clinicaltrials.gov/ct2/show/NCT00356980. A Phase I rrial of TNF-bound colloidal gold (CYT-6091) by intravenous administration in subjects with advanced solid organ malignancies. 2006.
12. [Accessed: April 30, 2016] https://clinicaltrials.gov/ct2/show/NCT00848042. a pilot study of aurolase(tm) therapy in patients with refractory and/or recurrent tumors of the head and neck. 2009.
13. [Accessed: April 30, 2016] https://clinicaltrials.gov/show/NCT02106598. targeted silica nanoparticles for image-guided intraoperative sentinel lymph node mapping in head and neck melanoma, breast and cervical/uterine cancer patients. 2014.
14. Ernsting MJ, Murakami M, Roy A, Li SD. Factors controlling the pharmacokinetics, biodistribution and intratumoral penetration of nanoparticles. J Control Release. 2013; 172:782–794. [PubMed: 24075927]
15. Choi HS, Liu W, Misra P, Tanaka E, Zimmer JP, Itty Ipe B, Bawendi MG, Frangioni JV. Renal clearance of quantum dots. Nat Biotechnol. 2007; 25:1165–1170. [PubMed: 17891134]
16. Chakravarty R, Hong H, Cai W. Positron emission tomography image-guided drug delivery: current status and future perspectives. Mol Pharm. 2014; 11:3777–3797. [PubMed: 24865108]
17. Zhou M, Song SL, Zhao J, Tian M, Li C. Theranostic CuS nanoparticles targeting folate receptors for PET image-guided photothermal therapy. J Mater Chem B. 2015; 3:8939–8948.
18. Pang B, Zhao Y, Luehmann H, Yang X, Detering L, You M, Zhang C, Zhang L, Li ZY, Ren Q, Liu Y, Xia Y. (6)(4)Cu-doped PdCu@Au tripods: A multifunctional nanomaterial for positron emission tomography and image-guided photothermal cancer treatment. ACS Nano. 2016; 10:3121–3131. [PubMed: 26824412]
19. Perez-Medina C, Abdel-Atti D, Tang J, Zhao Y, Fayad ZA, Lewis JS, Mulder WJ, Reiner T. Nanoreporter PET predicts the efficacy of anti-cancer nanotherapy. Nat Commun. 2016; 7
20. Goel S, Chen F, Ehlerding EB, Cai W. Intrinsically radiolabeled nanoparticles: an emerging paradigm. Small. 2014; 10:3825–3830. [PubMed: 24978934]
21. Sun X, Huang X, Yan X, Wang Y, Guo J, Jacobson O, Liu D, Szajek LP, Zhu W, Niu G, Kiesewetter DO, Sun S, Chen X. Chelator-free (64)Cu-integrated gold nanomaterials for positron emission tomography imaging guided photothermal cancer therapy. ACS Nano. 2014; 8:8438–8446. [PubMed: 25019252]
22. Shaffer TM, Wall MA, Harmsen S, Longo VA, Drain CM, Kircher MF, Grimm J. Silica nanoparticles as substrates for chelator-free labeling of oxophilic radioisotopes. Nano Lett. 2015; 15:864–868. [PubMed: 25559467]
23. Chen F, Goel S, Valdovinos HF, Luo H, Hernandez R, Barnhart TE, Cai W. In vivo integrity and biological fate of chelator-free Zirconium-89-labeled mesoporous silica nanoparticles. ACS Nano. 2015; 9:7950–7959. [PubMed: 26213260]
24. Chen F, Ellison PA, Lewis CM, Hong H, Zhang Y, Shi S, Hernandez R, Meyerand ME, Barnhart TE, Cai W. Chelator-free synthesis of a dual-modality PET/MRI agent. Angew Chem Int Ed Engl. 2013; 52:13319–13323. [PubMed: 24166933]

25. Chakravarty R, Valdovinos HF, Chen F, Lewis CM, Ellison PA, Luo H, Meyerand ME, Nickles RJ, Cai W. Intrinsically Germanium-69-labeled iron oxide nanoparticles: synthesis and in-vivo dual-modality PET/MR imaging. Adv Mater. 2014; 26:5119–5123. [PubMed: 24944166]
26. Sun Y, Liu Q, Peng J, Feng W, Zhang Y, Yang P, Li F. Radioisotope post-labeling upconversion nanophosphors for in vivo quantitative tracking. Biomaterials. 2013; 34:2289–2295. [PubMed: 23274071]
27. Liu Q, Sun Y, Li C, Zhou J, Yang T, Zhang X, Yi T, Wu D, Li F. 18F-Labeled magnetic-upconversion nanophosphors via rare-earth cation-assisted ligand assembly. ACS Nano. 2011; 5:3146–3157. [PubMed: 21384900]
28. Sun X, Huang X, Guo J, Zhu W, Ding Y, Niu G, Wang A, Kiesewetter DO, Wang ZL, Sun S, Chen X. Self-illuminating 64Cu-doped CdSe/ZnS nanocrystals for in vivo tumor imaging. J Am Chem Soc. 2014; 136:1706–1709. [PubMed: 24401138]
29. Perez-Campana C, Gomez-Vallejo V, Martin A, San Sebastian E, Moya SE, Reese T, Ziolo RF, Llop J. Tracing nanoparticles in vivo: a new general synthesis of positron emitting metal oxide nanoparticles by proton beam activation. The Analyst. 2012; 137:4902–4906. [PubMed: 22957337]
30. Perez-Campana C, Gomez-Vallejo V, Puigivila M, Martin A, Calvo-Fernandez T, Moya SE, Ziolo RF, Reese T, Llop J. Biodistribution of different sized nanoparticles assessed by positron emission tomography: a general strategy for direct activation of metal oxide particles. ACS Nano. 2013; 7:3498–3505. [PubMed: 23473535]
31. [Accessed: April 30, 2016] http://www.fda.gov/downloads/food/ingredientspackaginglabeling/gras/noticeinventory/ucm269494 Generally recognized as safe determination for silicon dioxide when added directly and/or indirectly to human food. 2010.
32. Vivero-Escoto JL, Huxford-Phillips RC, Lin W. Silica-based nanoprobes for biomedical imaging and theranostic applications. Chem Soc Rev. 2012; 41:2673–2685. [PubMed: 22234515]
33. Chen F, Hong H, Goel S, Graves SA, Orbay H, Ehlerding EB, Shi S, Theuer CP, Nickles RJ, Cai W. In vivo tumor vasculature targeting of CuS@MSN based theranostic nanomedicine. ACS Nano. 2015; 9:3926–3934. [PubMed: 25843647]
34. Burke BP, Baghdadi N, Clemente GS, Camus N, Guillou A, Kownacka AE, Domarkas J, Halime Z, Tripier R, Archibald SJ. Final step Gallium-68 radiolabelling of silica-coated iron oxide nanorods as potential PET/MR multimodal imaging agents. Farad Discuss. 2014; 175:59–71.
35. Burke BP, Baghdadi N, Kownacka AE, Nigam S, Clemente GS, Al-Yassiry MM, Domarkas J, Lorch M, Pickles M, Gibbs P, Tripier R, Cawthorne C, Archibald SJ. Chelator free Gallium-68 radiolabelling of silica coated iron oxide nanorods via surface interactions. Nanoscale. 2015; 7:14889–14896. [PubMed: 26292197]
36. Phillips E, Penate-Medina O, Zanzonico PB, Carvajal RD, Mohan P, Ye Y, Humm J, Gonen M, Kalaigian H, Schoder H, Strauss HW, Larson SM, Wiesner U, Bradbury MS. Clinical translation of an ultrasmall inorganic optical-PET imaging nanoparticle probe. Sci Transl Med. 2014; 6:260ra149.
37. Benezra M, Penate-Medina O, Zanzonico PB, Schaer D, Ow H, Burns A, DeStanchina E, Longo V, Herz E, Iyer S, Wolchok J, Larson SM, Wiesner U, Bradbury MS. Multimodal silica nanoparticles are effective cancer-targeted probes in a model of human melanoma. J Clin Invest. 2011; 121:2768–2780. [PubMed: 21670497]
38. Ma K, Mendoza C, Hanson M, Werner-Zwanziger U, Zwanziger J, Wiesner U. Control of ultrasmall sub-10 nm ligand-functionalized fluorescent core–shell silica nanoparticle growth in water. Chem Mater. 2015; 27:4119–4133.
39. Kumar R, Roy I, Ohulchanskky TY, Vathy LA, Bergey EJ, Sajjad M, Prasad PN. In vivo biodistribution and clearance studies using multimodal organically modified silica nanoparticles. ACS Nano. 2010; 4:699–708. [PubMed: 20088598]
40. Tang L, Yang X, Dobrucki LW, Chaudhury I, Yin Q, Yao C, Lezmi S, Helferich WG, Fan TM, Cheng J. Aptamer-functionalized, ultra-small, monodisperse silica nanoconjugates for targeted dual-modal imaging of lymph nodes with metastatic tumors. Angew Chem Int Ed Engl. 2012; 51:12721–12726. [PubMed: 23136130]

41. Vallet-Regi M, Rámila A, del Real RP, Pérez-Pariente J. A new property of MCM-41: Drug delivery system. Chem Mater. 2001; 13:308–311.
42. Tang F, Li L, Chen D. Mesoporous silica nanoparticles: synthesis, biocompatibility and drug delivery. Adv Mater. 2012; 24:1504–1534. [PubMed: 22378538]
43. Chen F, Hong H, Zhang Y, Valdovinos HF, Shi S, Kwon GS, Theuer CP, Barnhart TE, Cai W. In vivo tumor targeting and image-guided drug delivery with antibody-conjugated, radiolabeled mesoporous silica nanoparticles. ACS Nano. 2013; 7:9027–9039. [PubMed: 24083623]
44. Goel S, Chen F, Hong H, Valdovinos HF, Hernandez R, Shi S, Barnhart TE, Cai W. VEGF(1)(2)(1)-conjugated mesoporous silica nanoparticle: a tumor targeted drug delivery system. ACS Appl Mater Interfaces. 2014; 6:21677–21685. [PubMed: 25353068]
45. Chen F, Nayak TR, Goel S, Valdovinos HF, Hong H, Theuer CP, Barnhart TE, Cai W. In vivo tumor vasculature targeted PET/NIRF imaging with TRC105(Fab)-conjugated, dual-labeled mesoporous silica nanoparticles. Mol Pharm. 2014; 11:4007–4014. [PubMed: 24937108]
46. Lee SB, Kim HL, Jeong HJ, Lim ST, Sohn MH, Kim DW. Mesoporous silica nanoparticle pretargeting for PET imaging based on a rapid bioorthogonal reaction in a living body. Angew Chem Int Ed Engl. 2013; 52:10549–10552. [PubMed: 23956036]
47. Miller L, Winter G, Baur B, Witulla B, Solbach C, Reske S, Linden M. Synthesis, characterization, and biodistribution of multiple 89Zr-labeled pore-expanded mesoporous silica nanoparticles for PET. Nanoscale. 2014; 6:4928–4935. [PubMed: 24675844]
48. Qi G, Wang Y, Estevez L, Switzer AK, Duan X, Yang X, Giannelis EP. Facile and Scalable Synthesis of Monodispersed Spherical Capsules with a Mesoporous Shell. Chem Mater. 2010; 22:2693–2695.
49. Lin YS, Wu SH, Tseng CT, Hung Y, Chang C, Mou CY. Synthesis of hollow silica nanospheres with a microemulsion as the template. Chem Commun. 2009; 28:3542–3544.
50. Li L, Tang F, Liu H, Liu T, Hao N, Chen D, Teng X, He J. In vivo delivery of silica nanorattle encapsulated docetaxel for liver cancer therapy with low toxicity and high efficacy. ACS Nano. 2010; 4:6874–6882. [PubMed: 20973487]
51. Luo Z, Ding X, Hu Y, Wu S, Xiang Y, Zeng Y, Zhang B, Yan H, Zhang H, Zhu L, Liu J, Li J, Cai K, Zhao Y. Engineering a hollow nanocontainer platform with multifunctional molecular machines for tumor-targeted therapy in vitro and in vivo. ACS Nano. 2013; 7:10271–10284. [PubMed: 24127723]
52. Shi S, Chen F, Cai W. Biomedical applications of functionalized hollow mesoporous silica nanoparticles: focusing on molecular imaging. Nanomedicine. 2013; 8:2027–2039. [PubMed: 24279491]
53. Fan W, Shen B, Bu W, Chen F, Zhao K, Zhang S, Zhou L, Peng W, Xiao Q, Xing H, Liu J, Ni D, He Q, Shi J. Rattle-structured multifunctional nanotheranostics for synergetic chemo-/radiotherapy and simultaneous magnetic/luminescent dual-mode imaging. J Am Chem Soc. 2013; 135:6494–6503. [PubMed: 23574400]
54. Chen Y, Chen H, Sun Y, Zheng Y, Zeng D, Li F, Zhang S, Wang X, Zhang K, Ma M, He Q, Zhang L, Shi J. Multifunctional mesoporous composite nanocapsules for highly efficient MRI-guided high-intensity focused ultrasound cancer surgery. Angew Chem Int Ed Engl. 2011; 50:12505–12509. [PubMed: 22076783]
55. Chen F, Hong H, Shi S, Goel S, Valdovinos HF, Hernandez R, Theuer CP, Barnhart TE, Cai W. Engineering of hollow mesoporous silica nanoparticles for remarkably enhanced tumor active targeting efficacy. Sci Rep. 2014; 4
56. Al Faraj A, Alotaibi B, Shaik AP, Shamma KZ, Al Jammaz I, Gerl J. Sodium-22-radiolabeled silica nanoparticles as new radiotracer for biomedical applications: in vivo positron emission tomography imaging, biodistribution, and biocompatibility. Int J Nanomedicine. 2015; 10:6293–6302. [PubMed: 26504381]
57. Kroto HW, Heath JR, O'Brien SC, Curl RF, Smalley RE. C60: Buckminsterfullerene. Nature. 1985; 318:162–163.
58. Iijima S. Helical microtubules of graphitic carbon. Nature. 1991; 354:56–58.

59. Novoselov KS, Geim AK, Morozov SV, Jiang D, Zhang Y, Dubonos SV, Grigorieva IV, Firsov AA. Electric field effect in atomically thin carbon films. Science. 2004; 306:666–669. [PubMed: 15499015]
60. Xu X, Ray R, Gu Y, Ploehn HJ, Gearheart L, Raker K, Scrivens WA. Electrophoretic analysis and purification of fluorescent single-walled carbon nanotube fragments. J Am Chem Soc. 2004; 126:12736–12737. [PubMed: 15469243]
61. Baker SN, Baker GA. Luminescent carbon nanodots: emergent nanolights. Angew Chem Int Ed Engl. 2010; 49:6726–6744. [PubMed: 20687055]
62. Mochalin VN, Shenderova O, Ho D, Gogotsi Y. The properties and applications of nanodiamonds. Nat Nanotechnol. 2012; 7:11–23.
63. Hong G, Diao S, Antaris AL, Dai H. Carbon Nanomaterials for biological imaging and nanomedicinal therapy. Chem Rev. 2015; 115:10816–10906. [PubMed: 25997028]
64. Gong H, Peng R, Liu Z. Carbon nanotubes for biomedical imaging: the recent advances. Adv Drug Deliv Rev. 2013; 65:1951–1963. [PubMed: 24184130]
65. Yoo JM, Kang JH, Hong BH. Graphene-based nanomaterials for versatile imaging studies. Chem Soc Rev. 2015; 44:4835–4852. [PubMed: 25777530]
66. Welsher K, Liu Z, Sherlock SP, Robinson JT, Chen Z, Daranciang D, Dai H. A route to brightly fluorescent carbon nanotubes for near-infrared imaging in mice. Nat Nanotechnol. 2009; 4:773–780. [PubMed: 19893526]
67. Kim JW, Galanzha EI, Shashkov EV, Moon HM, Zharov VP. Golden carbon nanotubes as multimodal photoacoustic and photothermal high-contrast molecular agents. Nat Nanotechnol. 2009; 4:688–694. [PubMed: 19809462]
68. Yang K, Zhang S, Zhang G, Sun X, Lee ST, Liu Z. Graphene in mice: ultrahigh in vivo tumor uptake and efficient photothermal therapy. Nano Lett. 2010; 10:3318–3323. [PubMed: 20684528]
69. Liu Z, Li X, Tabakman SM, Jiang K, Fan S, Dai H. Multiplexed multicolor Raman imaging of live cells with isotopically modified single walled carbon nanotubes. J Am Chem Soc. 2008; 130:13540–13541. [PubMed: 18803379]
70. Malard LM, Pimenta MA, Dresselhaus G, Dresselhaus MS. Raman spectroscopy in graphene. Phys Rep. 2009; 473:51–87.
71. Shi S, Chen F, Ehlerding EB, Cai W. Surface engineering of graphene-based nanomaterials for biomedical applications. Bioconjug Chem. 2014; 25:1609–1619. [PubMed: 25117569]
72. Wang H, Wang J, Deng X, Sun H, Shi Z, Gu Z, Liu Y, Zhao Y. Biodistribution of carbon single-wall carbon nanotubes in mice. J Nanosci Nanotechnol. 2004; 4:1019–1024. [PubMed: 15656196]
73. Singh R, Pantarotto D, Lacerda L, Pastorin G, Klumpp C, Prato M, Bianco A, Kostarelos K. Tissue biodistribution and blood clearance rates of intravenously administered carbon nanotube radiotracers. Proc Natl Acad Sci USA. 2006; 103:3357–3362. [PubMed: 16492781]
74. Guo J, Zhang X, Li Q, Li W. Biodistribution of functionalized multiwall carbon nanotubes in mice. Nucl Med Biol. 2007; 34:579–583. [PubMed: 17591558]
75. McDevitt MR, Chattopadhyay D, Jaggi JS, Finn RD, Zanzonico PB, Villa C, Rey D, Mendenhall J, Batt CA, Njardarson JT, Scheinberg DA. PET imaging of soluble yttrium-86-labeled carbon nanotubes in mice. PloS One. 2007; 2:e907. [PubMed: 17878942]
76. Georgin D, Czarny B, Botquin M, Mayne-L'hermite M, Pinault M, Bouchet-Fabre B, Carriere M, Poncy JL, Chau Q, Maximilien R, Dive V, Taran F. Preparation of (14)C-labeled multiwalled carbon nanotubes for biodistribution investigations. J Am Chem Soc. 2009; 131:14658–14659. [PubMed: 19788249]
77. Czarny B, Georgin D, Berthon F, Plastow G, Pinault M, Patriarche G, Thuleau A, L'Hermite MM, Taran F, Dive V. Carbon nanotube translocation to distant organs after pulmonary exposure: insights from in situ (14)C-radiolabeling and tissue radioimaging. ACS Nano. 2014; 8:5715–5724. [PubMed: 24853551]
78. Liu Z, Cai W, He L, Nakayama N, Chen K, Sun X, Chen X, Dai H. In vivo biodistribution and highly efficient tumour targeting of carbon nanotubes in mice. Nat Nanotechnol. 2007; 2:47–52. [PubMed: 18654207]

79. McDevitt MR, Chattopadhyay D, Kappel BJ, Jaggi JS, Schiffman SR, Antczak C, Njardarson JT, Brentjens R, Scheinberg DA. Tumor targeting with antibody-functionalized, radiolabeled carbon nanotubes. J Nucl Med. 2007; 48:1180–1189. [PubMed: 17607040]

80. Ruggiero A, Villa CH, Holland JP, Sprinkle SR, May C, Lewis JS, Scheinberg DA, McDevitt MR. Imaging and treating tumor vasculature with targeted radiolabeled carbon nanotubes. Int J Nanomedicine. 2010; 5:783–802. [PubMed: 21042424]

81. Swierczewska M, Choi KY, Mertz EL, Huang X, Zhang F, Zhu L, Yoon HY, Park JH, Bhirde A, Lee S, Chen X. A facile, one-step nanocarbon functionalization for biomedical applications. Nano Lett. 2012; 12:3613–3620. [PubMed: 22694219]

82. Hong SY, Tobias G, Al-Jamal KT, Ballesteros B, Ali-Boucetta H, Lozano-Perez S, Nellist PD, Sim RB, Finucane C, Mather SJ, Green ML, Kostarelos K, Davis BG. Filled and glycosylated carbon nanotubes for in vivo radioemitter localization and imaging. Nat Mater. 2010; 9:485–490. [PubMed: 20473287]

83. Matson ML, Villa CH, Ananta JS, Law JJ, Scheinberg DA, Wilson LJ. Encapsulation of alpha-Particle-Emitting 225Ac3+ Ions Within Carbon Nanotubes. J Nucl Med. 2015; 56:897–900. [PubMed: 25931476]

84. Cisneros BT, Law JJ, Matson ML, Azhdarinia A, Sevick-Muraca EM, Wilson LJ. Stable confinement of positron emission tomography and magnetic resonance agents within carbon nanotubes for bimodal imaging. Nanomedicine (Lond). 2014; 9:2499–2509. [PubMed: 24628687]

85. Rong P, Yang K, Srivastan A, Kiesewetter DO, Yue X, Wang F, Nie L, Bhirde A, Wang Z, Liu Z, Niu G, Wang W, Chen X. Photosensitizer loaded nano-graphene for multimodality imaging guided tumor photodynamic therapy. Theranostics. 2014; 4:229–239. [PubMed: 24505232]

86. Yang K, Feng L, Shi X, Liu Z. Nano-graphene in biomedicine: theranostic applications. Chem Soc Rev. 2013; 42:530–547. [PubMed: 23059655]

87. Yang K, Feng L, Hong H, Cai W, Liu Z. Preparation and functionalization of graphene nanocomposites for biomedical applications. Nat Protoc. 2013; 8:2392–2403. [PubMed: 24202553]

88. Hong H, Yang K, Zhang Y, Engle JW, Feng L, Yang Y, Nayak TR, Goel S, Bean J, Theuer CP, Barnhart TE, Liu Z, Cai W. In vivo targeting and imaging of tumor vasculature with radiolabeled, antibody-conjugated nanographene. ACS Nano. 2012; 6:2361–2370. [PubMed: 22339280]

89. Xu C, Shi S, Feng L, Chen F, Graves SA, Ehlerding EB, Goel S, Sun H, England CG, Nickles RJ, Liu Z, Wang T, Cai W. Long circulating reduced graphene oxide-iron oxide nanoparticles for efficient tumor targeting and multimodality imaging. Nanoscale. 2016; 25:25.

90. Shi S, Yang K, Hong H, Chen F, Valdovinos HF, Goel S, Barnhart TE, Liu Z, Cai W. VEGFR targeting leads to significantly enhanced tumor uptake of nanographene oxide in vivo. Biomaterials. 2015; 39:39–46. [PubMed: 25477170]

91. Shi S, Yang K, Hong H, Valdovinos HF, Nayak TR, Zhang Y, Theuer CP, Barnhart TE, Liu Z, Cai W. Tumor vasculature targeting and imaging in living mice with reduced graphene oxide. Biomaterials. 2013; 34:3002–3009. [PubMed: 23374706]

92. Cornelissen B, Able S, Kersemans V, Waghorn PA, Myhra S, Jurkshat K, Crossley A, Vallis KA. Nanographene oxide-based radioimmunoconstructs for in vivo targeting and SPECT imaging of HER2-positive tumors. Biomaterials. 2013; 34:1146–1154. [PubMed: 23171545]

93. Hong H, Zhang Y, Engle JW, Nayak TR, Theuer CP, Nickles RJ, Barnhart TE, Cai W. In vivo targeting and positron emission tomography imaging of tumor vasculature with (66)Ga-labeled nano-graphene. Biomaterials. 2012; 33:4147–4156. [PubMed: 22386918]

94. Yang K, Wan J, Zhang S, Zhang Y, Lee ST, Liu Z. In vivo pharmacokinetics, long-term biodistribution, and toxicology of PEGylated graphene in mice. ACS Nano. 2011; 5:516–522. [PubMed: 21162527]

95. Jasim DA, Menard-Moyon C, Begin D, Bianco A, Kostarelos K. Tissue distribution and urinary excretion of intravenously administered chemically functionalized graphene oxide sheets. Chem Sci. 2015; 6:3952–3964. [PubMed: 28717461]

96. Song J, Yang X, Jacobson O, Lin L, Huang P, Niu G, Ma Q, Chen X. Sequential drug release and enhanced photothermal and photoacoustic effect of hybrid reduced graphene oxide-loaded

ultrasmall gold nanorod vesicles for cancer therapy. ACS Nano. 2015; 9:9199–9209. [PubMed: 26308265]

97. Chen L, Zhong X, Yi X, Huang M, Ning P, Liu T, Ge C, Chai Z, Liu Z, Yang K. Radionuclide (131)I labeled reduced graphene oxide for nuclear imaging guided combined radio- and photothermal therapy of cancer. Biomaterials. 2015; 66:21–28. [PubMed: 26188609]
98. Huang X, Zhang F, Zhu L, Choi KY, Guo N, Guo J, Tackett K, Anilkumar P, Liu G, Quan Q, Choi HS, Niu G, Sun YP, Lee S, Chen X. Effect of injection routes on the biodistribution, clearance, and tumor uptake of carbon dots. ACS Nano. 2013; 7:5684–5693. [PubMed: 23731122]
99. Rojas S, Gispert JD, Martin R, Abad S, Menchon C, Pareto D, Victor VM, Alvaro M, Garcia H, Herance JR. Biodistribution of amino-functionalized diamond nanoparticles. In vivo studies based on 18F radionuclide emission. ACS Nano. 2011; 5:5552–5559. [PubMed: 21657210]
100. Li J, Yang W, Cui R, Wang D, Chang Y, Gu W, Yin W, Bai X, Chen K, Xia L, Geng H, Xing G. Metabolizer in vivo of fullerenes and metallofullerenes by positron emission tomography. Nanotechnology. 2016; 27:155101. [PubMed: 26926042]
101. Chen M, Yin M. Design and development of fluorescent nanostructures for bioimaging. Prog Polym Sci. 2014; 39:365–395.
102. Wolfbeis OS. An overview of nanoparticles commonly used in fluorescent bioimaging. Chem Soc Rev. 2015; 44:4743–4768. [PubMed: 25620543]
103. Michalet X, Pinaud FF, Bentolila LA, Tsay JM, Doose S, Li JJ, Sundaresan G, Wu AM, Gambhir SS, Weiss S. Quantum dots for live cells, in vivo imaging, and diagnostics. Science. 2005; 307:538–544. [PubMed: 15681376]
104. Yang, SP., Goel, S., W, C. In vivo molecular imaging with quantum dots: toward multimodality and theranostics. In: Prokopovich, P., editor. Biological and pharmaceutical applications of nanomaterials. 2015. p. 319-346.CRC Press
105. Resch-Genger U, Grabolle M, Cavaliere-Jaricot S, Nitschke R, Nann T. Quantum dots versus organic dyes as fluorescent labels. Nat Methods. 2008; 5:763–775. [PubMed: 18756197]
106. Smith AM, Nie S. Semiconductor nanocrystals: structure, properties, and band gap engineering. Acc Chem Res. 2010; 43:190–200. [PubMed: 19827808]
107. Jin S, Hu YX, Gu ZJ, Liu L, Wu HC. Application of quantum dots in biological imaging. J Nanomater. 2011; 2011:13.
108. Huang HC, Barua S, Sharma G, Dey SK, Rege K. Inorganic nanoparticles for cancer imaging and therapy. J Control Release. 2011; 155:344–357. [PubMed: 21723891]
109. Medintz IL, Uyeda HT, Goldman ER, Mattoussi H. Quantum dot bioconjugates for imaging, labelling and sensing. Nat Mater. 2005; 4:435–446. [PubMed: 15928695]
110. Robe A, Pic E, Lassalle HP, Bezdetnaya L, Guillemin F, Marchal F. Quantum dots in axillary lymph node mapping: biodistribution study in healthy mice. BMC Cancer. 2008; 8:111. [PubMed: 18430208]
111. Cai W, Chen K, Li ZB, Gambhir SS, Chen X. Dual-function probe for PET and near-infrared fluorescence imaging of tumor vasculature. J Nucl Med. 2007; 48:1862–1870. [PubMed: 17942800]
112. Duconge F, Pons T, Pestourie C, Herin L, Theze B, Gombert K, Mahler B, Hinnen F, Kuhnast B, Dolle F, Dubertret B, Tavitian B. Fluorine-18-labeled phospholipid quantum dot micelles for in vivo multimodal imaging from whole body to cellular scales. Bioconjug Chem. 2008; 19:1921–1926. [PubMed: 18754572]
113. Chen K, Li ZB, Wang H, Cai W, Chen X. Dual-modality optical and positron emission tomography imaging of vascular endothelial growth factor receptor on tumor vasculature using quantum dots. Eur J Nucl Med Mol Imaging. 2008; 35:2235–2244. [PubMed: 18566815]
114. Tu C, Ma X, House A, Kauzlarich SM, Louie AY. PET imaging and biodistribution of silicon quantum dots in mice. ACS Med Chem Lett. 2011; 2:285–288. [PubMed: 21546997]
115. Hu K, Wang H, Tang G, Huang T, Tang X, Liang X, Yao S, Nie D. In vivo cancer dual-targeting and dual-modality imaging with functionalized quantum dots. J Nucl Med. 2015; 56:1278–1284. [PubMed: 26112023]
116. Schipper ML, Iyer G, Koh AL, Cheng Z, Ebenstein Y, Aharoni A, Keren S, Bentolila LA, Li J, Rao J, Chen X, Banin U, Wu AM, Sinclair R, Weiss S, Gambhir SS. Particle size, surface

coating, and PEGylation influence the biodistribution of quantum dots in living mice. Small. 2009; 5:126–134. [PubMed: 19051182]

117. Schipper ML, Cheng Z, Lee SW, Bentolila LA, Iyer G, Rao J, Chen X, Wu AM, Weiss S, Gambhir SS. microPET-based biodistribution of quantum dots in living mice. J Nucl Med. 2007; 48:1511–1518. [PubMed: 17704240]
118. Cai W, Hong H. In a "nutshell": intrinsically radio-labeled quantum dots. Am J Nucl Med Mol Imaging. 2012; 2:136–140. [PubMed: 23133808]
119. Woodward JD, Kennel SJ, Mirzadeh S, Dai S, Wall JS, Richey T, Avenell J, Rondinone AJ. In vivo SPECT/CT imaging and biodistribution using radioactive Cd125mTe/ZnS nanoparticles. Nanotechnology. 2007; 18:175103.
120. Kennel SJ, Woodward JD, Rondinone AJ, Wall J, Huang Y, Mirzadeh S. The fate of MAb-targeted Cd(125m)Te/ZnS nanoparticles in vivo. Nucl Med Biol. 2008; 35:501–514. [PubMed: 18482688]
121. Sun M, Hoffman D, Sundaresan G, Yang L, Lamichhane N, Zweit J. Synthesis and characterization of intrinsically radiolabeled quantum dots for bimodal detection. Am J Nucl Med Mol Imaging. 2012; 2:122–135. [PubMed: 23133807]
122. Guo W, Sun X, Jacobson O, Yan X, Min K, Srivatsan A, Niu G, Kiesewetter DO, Chang J, Chen X. Intrinsically radioactive [64Cu]CuInS/ZnS quantum dots for PET and optical imaging: improved radiochemical stability and controllable Cerenkov luminescence. ACS Nano. 2015; 9:488–495. [PubMed: 25549258]
123. Li J, Dobrucki LW, Marjanovic M, Chaney EJ, Suslick KS, Boppart SA. Enhancement and wavelength-shifted emission of Cerenkov luminescence using multifunctional microspheres. Phys Med Biol. 2015; 60:727–739. [PubMed: 25555157]
124. Boschi F, Spinelli AE. Quantum dots excitation using pure beta minus radioisotopes emitting Cerenkov radiation. RSC Adv. 2012; 2:11049–11052.
125. Dothager RS, Goiffon RJ, Jackson E, Harpstrite S, Piwnica-Worms D. Cerenkov radiation energy transfer (CRET) imaging: a novel method for optical imaging of PET isotopes in biological systems. PloS One. 2010; 5:0013300.
126. Shen J, Zhao L, Han G. Lanthanide-doped upconverting luminescent nanoparticle platforms for optical imaging-guided drug delivery and therapy. Adv Drug Deliv Rev. 2013; 65:744–755. [PubMed: 22626980]
127. Gu Z, Yan L, Tian G, Li S, Chai Z, Zhao Y. Recent advances in design and fabrication of upconversion nanoparticles and their safe theranostic applications. Adv Mater. 2013; 25:3758–3779. [PubMed: 23813588]
128. Nam J, Won N, Bang J, Jin H, Park J, Jung S, Park Y, Kim S. Surface engineering of inorganic nanoparticles for imaging and therapy. Adv Drug Deliv Rev. 2013; 65:622–648. [PubMed: 22975010]
129. Park YI, Lee KT, Suh YD, Hyeon T. Upconverting nanoparticles: a versatile platform for wide-field two-photon microscopy and multi-modal in vivo imaging. Chem Soc Rev. 2015; 44:1302–1317. [PubMed: 25042637]
130. Zhou J, Liu Z, Li F. Upconversion nanophosphors for small-animal imaging. Chem Soc Rev. 2012; 41:1323–1349. [PubMed: 22008740]
131. Chen G, Qiu H, Prasad PN, Chen X. Upconversion nanoparticles: design, nanochemistry, and applications in theranostics. Chem Rev. 2014; 114:5161–5214. [PubMed: 24605868]
132. Janowski M, Bulte JW, Walczak P. Personalized nanomedicine advancements for stem cell tracking. Adv Drug Deliv Rev. 2012; 64:1488–1507. [PubMed: 22820528]
133. Wang C, Cheng L, Liu Z. Upconversion nanoparticles for photodynamic therapy and other cancer therapeutics. Theranostics. 2013; 3:317–330. [PubMed: 23650479]
134. Liu F, He X, Lei Z, Liu L, Zhang J, You H, Zhang H, Wang Z. Facile preparation of doxorubicin-loaded upconversion@polydopamine nanoplatforms for simultaneous in vivo multimodality imaging and chemophotothermal synergistic therapy. Adv Healthc Mater. 2015; 4:559–568. [PubMed: 25471617]

135. Chen Q, Wang C, Cheng L, He W, Cheng Z, Liu Z. Protein modified upconversion nanoparticles for imaging-guided combined photothermal and photodynamic therapy. Biomaterials. 2014; 35:2915–2923. [PubMed: 24412081]
136. Yuan Y, Min Y, Hu Q, Xing B, Liu B. NIR photoregulated chemo- and photodynamic cancer therapy based on conjugated polyelectrolyte-drug conjugate encapsulated upconversion nanoparticles. Nanoscale. 2014; 6:11259–11272. [PubMed: 25130329]
137. Chen F, Bu W, Cai W, Shi J. Functionalized upconversion nanoparticles: versatile nanoplatforms for translational research. Curr Mol Med. 2013; 13:1613–1632. [PubMed: 24206131]
138. Gallo J, Alam IS, Jin J, Gu YJ, Aboagye EO, Wong WT, Long NJ. PET imaging with multimodal upconversion nanoparticles. Dalton Trans. 2014; 43:5535–5545. [PubMed: 24535647]
139. Seo HJ, Nam SH, Im HJ, Park JY, Lee JY, Yoo B, Lee YS, Jeong JM, Hyeon T, Kim JW, Lee JS, Jang IJ, Cho JY, Hwang do W, Suh YD, Lee DS. Rapid hepatobiliary excretion of micelle-encapsulated/radiolabeled upconverting nanoparticles as an integrated form. Sci Rep. 2015; 5:15685. [PubMed: 26494465]
140. Rieffel J, Chen F, Kim J, Chen G, Shao W, Shao S, Chitgupi U, Hernandez R, Graves SA, Nickles RJ, Prasad PN, Kim C, Cai W, Lovell JF. Hexamodal imaging with porphyrin-phospholipid-coated upconversion nanoparticles. Adv Mater. 2015; 27:1785–1790. [PubMed: 25640213]
141. Lee J, Lee TS, Ryu J, Hong S, Kang M, Im K, Kang JH, Lim SM, Park S, Song R. RGD peptide-conjugated multimodal NaGdF4:Yb3+/Er3+ nanophosphors for upconversion luminescence, MR, and PET imaging of tumor angiogenesis. J Nucl Med. 2013; 54:96–103. [PubMed: 23232276]
142. Cao T, Yang Y, Sun Y, Wu Y, Gao Y, Feng W, Li F. Biodistribution of sub-10 nm PEG-modified radioactive/upconversion nanoparticles. Biomaterials. 2013; 34:7127–7134. [PubMed: 23796579]
143. Peng J, Sun Y, Zhao L, Wu Y, Feng W, Gao Y, Li F. Polyphosphoric acid capping radioactive/upconverting NaLuF4:Yb,Tm,153Sm nanoparticles for blood pool imaging in vivo. Biomaterials. 2013; 34:9535–9544. [PubMed: 24011713]
144. Sun Y, Zhu X, Peng J, Li F. Core-shell lanthanide upconversion nanophosphors as four-modal probes for tumor angiogenesis imaging. ACS Nano. 2013; 7:11290–11300. [PubMed: 24205939]
145. Yang Y, Sun Y, Cao T, Peng J, Liu Y, Wu Y, Feng W, Zhang Y, Li F. Hydrothermal synthesis of NaLuF4:153Sm,Yb,Tm nanoparticles and their application in dual-modality upconversion luminescence and SPECT bioimaging. Biomaterials. 2013; 34:774–783. [PubMed: 23117216]
146. Sun Y, Yu M, Liang S, Zhang Y, Li C, Mou T, Yang W, Zhang X, Li B, Huang C, Li F. Fluorine-18 labeled rare-earth nanoparticles for positron emission tomography (PET) imaging of sentinel lymph node. Biomaterials. 2011; 32:2999–3007. [PubMed: 21295345]
147. Zhou J, Yu M, Sun Y, Zhang X, Zhu X, Wu Z, Wu D, Li F. Fluorine-18-labeled Gd3+/Yb3+/Er3+ co-doped NaYF4 nanophosphors for multimodality PET/MR/UCL imaging. Biomaterials. 2011; 32:1148–1156. [PubMed: 20965563]
148. Liu Q, Chen M, Sun Y, Chen G, Yang T, Gao Y, Zhang X, Li F. Multifunctional rare-earth self-assembled nanosystem for tri-modal upconversion luminescence /fluorescence /positron emission tomography imaging. Biomaterials. 2011; 32:8243–8253. [PubMed: 21820170]
149. Wu JZ, Dai J, Shao YB, Sun YC. One-step synthesis of fluorescent silicon quantum dots (Si-QDs) and their application for cell imaging. RSC Adv. 2015; 5:83581–83587.
150. Erogbogbo F, Yong KT, Roy I, Xu G, Prasad PN, Swihart MT. Biocompatible luminescent silicon quantum dots for imaging of cancer cells. ACS Nano. 2008; 2:873–878. [PubMed: 19206483]
151. Erogbogbo F, Tien CA, Chang CW, Yong KT, Law WC, Ding H, Roy I, Swihart MT, Prasad PN. Bioconjugation of luminescent silicon quantum dots for selective uptake by cancer cells. Bioconjug Chem. 2011; 22:1081–1088. [PubMed: 21473652]
152. Zhao F, Li Z, Wang L, Hu C, Zhang Z, Li C, Qu L. Supramolecular quantum dots as biodegradable nano-probes for upconversion-enabled bioimaging. Chem Commun. 2015; 51:13201–13204.
153. Gargas DJ, Chan EM, Ostrowski AD, Aloni S, Altoe MV, Barnard ES, Sanii B, Urban JJ, Milliron DJ, Cohen BE, Schuck PJ. Engineering bright sub-10-nm upconverting nanocrystals for single-molecule imaging. Nat Nanotechnol. 2014; 9:300–305. [PubMed: 24633523]

154. Yang D, Dai Y, Liu J, Zhou Y, Chen Y, Li C, Ma P, Lin J. Ultra-small BaGdF5-based upconversion nanoparticles as drug carriers and multimodal imaging probes. Biomaterials. 2014; 35:2011–2023. [PubMed: 24314558]

155. Huang HC, Ramos J, Grandhi TSP, Potta T, Rege K. Gold Nanoparticles in cancer imaging and therapeutics. Nano Life. 2010; 01:289–307.

156. Jiao PF, Zhou HY, Chen LX, Yan B. Cancer-targeting multifunctionalized gold nanoparticles in imaging and therapy. Curr Med Chem. 2011; 18:2086–2102. [PubMed: 21517767]

157. Deb S, Ghosh K, Shetty SD. Nanoimaging in cardiovascular diseases: Current state of the art. Indian J Med Res. 2015; 141:285–298. [PubMed: 25963489]

158. Spivak MY, Bubnov RV, Yemets IM, Lazarenko LM, Tymoshok NO, Ulberg ZR. Gold nanoparticles - the theranostic challenge for PPPM: nanocardiology application. EPMA J. 2013; 4:18. [PubMed: 23800174]

159. Stendahl JC, Sinusas AJ. Nanoparticles for cardiovascular imaging and therapeutic delivery, Part 2: Radiolabeled probes. J Nucl Med. 2015; 56:1637–1641. [PubMed: 26294304]

160. Wan XY, Zheng LL, Gao PF, Yang XX, Li CM, Li YF, Huang CZ. Real-time light scattering tracking of gold nanoparticles- bioconjugated respiratory syncytial virus infecting HEP-2 cells. Sci Rep. 2014; 4:4529. [PubMed: 24681709]

161. Wang T, Zhang Z, Gao D, Li F, Wei H, Liang X, Cui Z, Zhang XE. Encapsulation of gold nanoparticles by simian virus 40 capsids. Nanoscale. 2011; 3:4275–4282. [PubMed: 21879117]

162. Lee JH, Oh BK, Choi JW. Development of a HIV-1 virus detection system based on nanotechnology. Sensors (Basel). 2015; 15:9915–9927. [PubMed: 25923937]

163. Dykman L, Khlebtsov N. Gold nanoparticles in biomedical applications: recent advances and perspectives. Chem Soc Rev. 2012; 41:2256–2282. [PubMed: 22130549]

164. Daniel MC, Astruc D. Gold nanoparticles: assembly, supramolecular chemistry, quantum-size-related properties, and applications toward biology, catalysis, and nanotechnology. Chem Rev. 2004; 104:293–346. [PubMed: 14719978]

165. Zhang X. Gold nanoparticles: Recent advances in the biomedical applications. Cell Biochem Biophys. 2015

166. Lai SF, Ko BH, Chien CC, Chang CJ, Yang SM, Chen HH, Petibois C, Hueng DY, Ka SM, Chen A, Margaritondo G, Hwu Y. Gold nanoparticles as multimodality imaging agents for brain gliomas. J Nanobiotechnology. 2015; 13:85. [PubMed: 26589283]

167. Huang X, El-Sayed MA. Gold nanoparticles: Optical properties and implementations in cancer diagnosis and photothermal therapy. J Adv Res. 2010; 1:13–28.

168. Jain S, Hirst DG, O'Sullivan JM. Gold nanoparticles as novel agents for cancer therapy. Br J Radiol. 2012; 85:101–113. [PubMed: 22010024]

169. Huang X, Jain PK, El-Sayed IH, El-Sayed MA. Plasmonic photothermal therapy (PPTT) using gold nanoparticles. Lasers Med Sci. 2008; 23:217–228. [PubMed: 17674122]

170. Young JK, Figueroa ER, Drezek RA. Tunable nanostructures as photothermal theranostic agents. Ann Biomed Eng. 2012; 40:438–459. [PubMed: 22134466]

171. Bazak R, Houri M, El Achy S, Kamel S, Refaat T. Cancer active targeting by nanoparticles: a comprehensive review of literature. J Cancer Res Clin Oncol. 2015; 141:769–784. [PubMed: 25005786]

172. Liu Y, Yuan H, Fales AM, Register JK, Vo-Dinh T. Multifunctional gold nanostars for molecular imaging and cancer therapy. Front Chem. 2015; 3:51. [PubMed: 26322306]

173. Bertrand N, Wu J, Xu X, Kamaly N, Farokhzad OC. Cancer nanotechnology: the impact of passive and active targeting in the era of modern cancer biology. Adv Drug Deliv Rev. 2014; 66:2–25. [PubMed: 24270007]

174. Kim B, Han G, Toley BJ, Kim CK, Rotello VM, Forbes NS. Tuning payload delivery in tumour cylindroids using gold nanoparticles. Nat Nanotechnol. 2010; 5:465–472. [PubMed: 20383126]

175. Pissuwan D, Niidome T, Cortie MB. The forthcoming applications of gold nanoparticles in drug and gene delivery systems. J Control Release. 2011; 149:65–71. [PubMed: 20004222]

176. Ajnai G, Chiu A, Kan T, Cheng C-C, Tsai T-H, Chang J. Trends of gold nanoparticle-based drug delivery system in cancer therapy. J Exp Clin Med. 2014; 6:172–178.

177. Han G, Ghosh P, Rotello VM. Functionalized gold nanoparticles for drug delivery. Nanomedicine (Lond). 2007; 2:113–123. [PubMed: 17716197]

178. Xing Y, Zhao J, Conti PS, Chen K. Radiolabeled nanoparticles for multimodality tumor imaging. Theranostics. 2014; 4:290–306. [PubMed: 24505237]

179. Li W, Sun X, Wang Y, Niu G, Chen X, Qian Z, Nie L. In vivo quantitative photoacoustic microscopy of gold nanostar kinetics in mouse organs. Biomed Opt Express. 2014; 5:2679–2685. [PubMed: 25136493]

180. Liu Y, Yuan H, Kersey FR, Register JK, Parrott MC, Vo-Dinh T. Plasmonic gold nanostars for multi-modality sensing and diagnostics. Sensors (Basel). 2015; 15:3706–3720. [PubMed: 25664431]

181. Liu Y, Ashton JR, Moding EJ, Yuan H, Register JK, Fales AM, Choi J, Whitley MJ, Zhao X, Qi Y, Ma Y, Vaidyanathan G, Zalutsky MR, Kirsch DG, Badea CT, Vo-Dinh T. A plasmonic gold nanostar theranostic probe for in vivo tumor imaging and photothermal therapy. Theranostics. 2015; 5:946–960. [PubMed: 26155311]

182. Pallavicini P, Bernhard C, Chirico G, Dacarro G, Denat F, Dona A, Milanese C, Taglietti A. Gold nanostars co-coated with the Cu(II) complex of a tetraazamacrocyclic ligand. Dalton Trans. 2015; 44:5652–5661. [PubMed: 25708886]

183. Peiris PM, Bauer L, Toy R, Tran E, Pansky J, Doolittle E, Schmidt E, Hayden E, Mayer A, Keri RA, Griswold MA, Karathanasis E. Enhanced delivery of chemotherapy to tumors using a multicomponent nanochain with radio-frequency-tunable drug release. ACS Nano. 2012; 6:4157–4168. [PubMed: 22486623]

184. Geng Y, Dalhaimer P, Cai S, Tsai R, Tewari M, Minko T, Discher DE. Shape effects of filaments versus spherical particles in flow and drug delivery. Nat Nanotechnol. 2007; 2:249–255. [PubMed: 18654271]

185. Zhang S, Gao H, Bao G. Physical Principles of Nanoparticle Cellular Endocytosis. ACS Nano. 2015; 9:8655–8671. [PubMed: 26256227]

186. Oh N, Park JH. Endocytosis and exocytosis of nanoparticles in mammalian cells. Int J Nanomedicine. 2014; 9(Suppl 1):51–63. [PubMed: 24872703]

187. Decuzzi P, Causa F, Ferrari M, Netti PA. The effective dispersion of nanovectors within the tumor microvasculature. Ann Biomed Eng. 2006; 34:633–641. [PubMed: 16568349]

188. Toy R, Hayden E, Camann A, Berman Z, Vicente P, Tran E, Meyers J, Pansky J, Peiris PM, Wu H, Exner A, Wilson D, Ghaghada KB, Karathanasis E. Multimodal in vivo imaging exposes the voyage of nanoparticles in tumor microcirculation. ACS Nano. 2013; 7:3118–3129. [PubMed: 23464827]

189. Morales-Avila E, Ferro-Flores G, Ocampo-García BE, De León-Rodríguez LM, Santos-Cuevas CL, García-Becerra R, Medina LA, Gómez-Oliván L. Multimeric system of 99mTc-labeled gold nanoparticles conjugated to c[RGDfK(C)] for molecular imaging of tumor α(v)β(3) expression. Bioconjug Chem. 2011; 22:913–922. [PubMed: 21513349]

190. Black KC, Akers WJ, Sudlow G, Xu B, Laforest R, Achilefu S. Dual-radiolabeled nanoparticle SPECT probes for bioimaging. Nanoscale. 2015; 7:440–444. [PubMed: 25418982]

191. Jang B, Park S, Kang SH, Kim JK, Kim SK, Kim IH, Choi Y. Gold nanorods for target selective SPECT/CT imaging and photothermal therapy in vivo. Quant Imaging Med Surg. 2012; 2:1–11. [PubMed: 23256055]

192. Xie H, Wang ZJ, Bao A, Goins B, Phillips WT. In vivo PET imaging and biodistribution of radiolabeled gold nanoshells in rats with tumor xenografts. Int J Pharm. 2010; 395:324–330. [PubMed: 20540999]

193. Xie H, Goins B, Bao A, Wang ZJ, Phillips WT. Effect of intratumoral administration on biodistribution of 64Cu-labeled nanoshells. Int J Nanomedicine. 2012; 7:2227–2238. [PubMed: 22619558]

194. Xie H, Diagaradjane P, Deorukhkar AA, Goins B, Bao A, Phillips WT, Wang Z, Schwartz J, Krishnan S. Integrin alphavbeta3-targeted gold nanoshells augment tumor vasculature-specific imaging and therapy. Int J Nanomedicine. 2011; 6:259–269. [PubMed: 21423588]

195. Bhatnagar P, Li Z, Choi Y, Guo J, Li F, Lee DY, Figliola M, Huls H, Lee DA, Zal T, Li KC, Cooper LJ. Imaging of genetically engineered T cells by PET using gold nanoparticles complexed to Copper-64. Integr Biol (Camb). 2013; 5:231–238. [PubMed: 23034721]
196. Karmani L, Bouchat V, Bouzin C, Leveque P, Labar D, Bol A, Deumer G, Marega R, Bonifazi D, Haufroid V, Michiels C, Gregoire V, Feron O, Lucas S, Vander Borght T, Gallez B. (89)Zr-labeled anti-endoglin antibody-targeted gold nanoparticles for imaging cancer: implications for future cancer therapy. Nanomedicine (London). 2014; 9:1923–1937.
197. Karmani L, Labar D, Valembois V, Bouchat V, Nagaswaran PG, Bol A, Gillart J, Leveque P, Bouzin C, Bonifazi D, Michiels C, Feron O, Gregoire V, Lucas S, Vander Borght T, Gallez B. Antibody-functionalized nanoparticles for imaging cancer: influence of conjugation to gold nanoparticles on the biodistribution of 89Zr-labeled cetuximab in mice. Contrast Media Mol Imaging. 2013; 8:402–408. [PubMed: 23740810]
198. Zhang Z, Liu Y, Jarreau C, Welch MJ, Taylor JS. Nucleic Acid-directed Self-assembly of multifunctional gold nanoparticle imaging agents. Biomater Sci. 2013; 1:1055–1064. [PubMed: 24058728]
199. Tian M, Lu W, Zhang R, Xiong C, Ensor J, Nazario J, Jackson J, Shaw C, Dixon KA, Miller J, Wright K, Li C, Gupta S. Tumor uptake of hollow gold nanospheres after intravenous and intra-arterial injection: PET/CT study in a rabbit VX2 liver cancer model. Mol Imaging Biol. 2013; 15:614–624. [PubMed: 23608932]
200. Li H, Diaz L, Lee D, Cui L, Liang X, Cheng Y. In vivo imaging of T cells loaded with gold nanoparticles: a pilot study. Radiol Med. 2014; 119:269–276. [PubMed: 24311191]
201. Wang Y, Liu Y, Luehmann H, Xia X, Brown P, Jarreau C, Welch M, Xia Y. Evaluating the pharmacokinetics and in vivo cancer targeting capability of Au nanocages by positron emission tomography imaging. ACS Nano. 2012; 6:5880–5888. [PubMed: 22690722]
202. Xiao Y, Hong H, Matson VZ, Javadi A, Xu W, Yang Y, Zhang Y, Engle JW, Nickles RJ, Cai W, Steeber DA, Gong S. Gold Nanorods Conjugated with Doxorubicin and cRGD for Combined Anticancer Drug Delivery and PET Imaging. Theranostics. 2012; 2:757–768. [PubMed: 22916075]
203. Cheng K, Kothapalli SR, Liu H, Koh AL, Jokerst JV, Jiang H, Yang M, Li J, Levi J, Wu JC, Gambhir SS, Cheng Z. Construction and validation of nano gold tripods for molecular imaging of living subjects. J Am Chem Soc. 2014; 136:3560–3571. [PubMed: 24495038]
204. Yang M, Cheng K, Qi S, Liu H, Jiang Y, Jiang H, Li J, Chen K, Zhang H, Cheng Z. Affibody modified and radiolabeled gold-iron oxide hetero-nanostructures for tumor PET, optical and MR imaging. Biomaterials. 2013; 34:2796–2806. [PubMed: 23343632]
205. Frigell J, Garcia I, Gomez-Vallejo V, Llop J, Penades S. 68Ga-labeled gold glyconanoparticles for exploring blood-brain barrier permeability: preparation, biodistribution studies, and improved brain uptake via neuropeptide conjugation. J Am Chem Soc. 2014; 136:449–457. [PubMed: 24320878]
206. Chen F, Goel S, Hernandez R, Graves SA, Shi S, Nickles RJ, Cai W. Dynamic positron emission tomography imaging of renal clearable gold nanoparticles. Small. 2016; 12:2775–2782. [PubMed: 27062146]
207. Abdelhalim MA. Alterations in gold nanoparticle levels are size dependent, with the smaller ones inducing the most toxic effects and related to the time of exposure of the gold nanoparticles. West Indian Med J. 2015; 65
208. Roy K, Lahiri S. A green method for synthesis of radioactive gold nanoparticles. Green Chem. 2006; 8:1063–1066.
209. Chanda N, Kattumuri V, Shukla R, Zambre A, Katti K, Upendran A, Kulkarni RR, Kan P, Fent GM, Casteel SW, Smith CJ, Boote E, Robertson JD, Cutler C, Lever JR, Katti KV, Kannan R. Bombesin functionalized gold nanoparticles show in vitro and in vivo cancer receptor specificity. Proc Natl Acad Sci USA. 2010; 107:8760–8765. [PubMed: 20410458]
210. Zhou C, Hao G, Thomas P, Liu J, Yu M, Sun S, Oz OK, Sun X, Zheng J. Near-infrared emitting radioactive gold nanoparticles with molecular pharmacokinetics. Angew Chem Int Ed Engl. 2012; 51:10118–10122. [PubMed: 22961978]

211. Wang Y, Liu Y, Luehmann H, Xia X, Wan D, Cutler C, Xia Y. Radioluminescent gold nanocages with controlled radioactivity for real-time in vivo imaging. Nano Lett. 2013; 13:581–585. [PubMed: 23360442]

212. Black KC, Wang Y, Luehmann HP, Cai X, Xing W, Pang B, Zhao Y, Cutler CS, Wang LV, Liu Y, Xia Y. Radioactive 198Au-doped nanostructures with different shapes for in vivo analyses of their biodistribution, tumor uptake, and intratumoral distribution. ACS Nano. 2014; 8:4385–4394. [PubMed: 24766522]

213. Zhao Y, Sultan D, Detering L, Cho S, Sun G, Pierce R, Wooley KL, Liu Y. Copper-64-alloyed gold nanoparticles for cancer imaging: improved radiolabel stability and diagnostic accuracy. Angew Chem Int Ed Engl. 2014; 53:156–159. [PubMed: 24272951]

214. Hu H, Huang P, Weiss OJ, Yan X, Yue X, Zhang MG, Tang Y, Nie L, Ma Y, Niu G, Wu K, Chen X. PET and NIR optical imaging using self-illuminating (64)Cu-doped chelator-free gold nanoclusters. Biomaterials. 2014; 35:9868–9876. [PubMed: 25224367]

215. Zhao Y, Sultan D, Detering L, Luehmann H, Liu Y. Facile synthesis, pharmacokinetic and systemic clearance evaluation, and positron emission tomography cancer imaging of (6)(4)Cu-Au alloy nanoclusters. Nanoscale. 2014; 6:13501–13509. [PubMed: 25266128]

216. Liu J, Yu M, Zhou C, Yang S, Ning X, Zheng J. Passive tumor targeting of renal-clearable luminescent gold nanoparticles: long tumor retention and fast normal tissue clearance. J Am Chem Soc. 2013; 135:4978–4981. [PubMed: 23506476]

217. McCarthy JR, Weissleder R. Multifunctional magnetic nanoparticles for targeted imaging and therapy. Adv Drug Deliv Rev. 2008; 60:1241–1251. [PubMed: 18508157]

218. Ohgushi M, Nagayama K, Wada A. Dextran-magnetite: A new relaxation reagent and its application to T2 measurements in gel systems. J Magn Reson (1969). 1978; 29:599–601.

219. Quick HH. Integrated PET/MR. J Magn Reson Imaging. 2014; 39:243–258. [PubMed: 24338921]

220. Wehrl HF, Sauter AW, Divine MR, Pichler BJ. Combined PET/MR: a technology becomes mature. J Nucl Med. 2015; 56:165–168. [PubMed: 25593114]

221. Bouziotis P, Psimadas D, Tsotakos T, Stamopoulos D, Tsoukalas C. Radiolabeled iron oxide nanoparticles as dual-modality SPECT/MRI and PET/MRI agents. Curr Top Med Chem. 2012; 12:2694–2702. [PubMed: 23339765]

222. Shao Y, Cherry SR, Farahani K, Meadors K, Siegel S, Silverman RW, Marsden PK. Simultaneous PET and MR imaging. Phys Med Biol. 1997; 42:1965–1970. [PubMed: 9364592]

223. Higuchi T, Nekolla SG, Jankaukas A, Weber AW, Huisman MC, Reder S, Ziegler SI, Schwaiger M, Bengel FM. Characterization of normal and infarcted rat myocardium using a combination of small-animal PET and clinical MRI. J Nucl Med. 2007; 48:288–294. [PubMed: 17268027]

224. Laurent S, Forge D, Port M, Roch A, Robic C, Vander Elst L, Muller RN. Magnetic iron oxide nanoparticles: synthesis, stabilization, vectorization, physicochemical characterizations, and biological applications. Chem Rev. 2008; 108:2064–2110. [PubMed: 18543879]

225. Kim J, Piao Y, Hyeon T. Multifunctional nanostructured materials for multimodal imaging, and simultaneous imaging and therapy. Chem Soc Rev. 2009; 38:372–390. [PubMed: 19169455]

226. Shubayev VI, Pisanic TR 2nd, Jin S. Magnetic nanoparticles for theragnostics. Adv Drug Deliv Rev. 2009; 61:467–477. [PubMed: 19389434]

227. Sun C, Lee JS, Zhang M. Magnetic nanoparticles in MR imaging and drug delivery. Adv Drug Deliv Rev. 2008; 60:1252–1265. [PubMed: 18558452]

228. Lee N, Hyeon T. Designed synthesis of uniformly sized iron oxide nanoparticles for efficient magnetic resonance imaging contrast agents. Chem Soc Rev. 2012; 41:2575–2589. [PubMed: 22138852]

229. De M, Chou SS, Joshi HM, Dravid VP. Hybrid magnetic nanostructures (MNS) for magnetic resonance imaging applications. Adv Drug Deliv Rev. 2011; 63:1282–1299. [PubMed: 21851844]

230. Kievit FM, Zhang M. Surface engineering of iron oxide nanoparticles for targeted cancer therapy. Acc Chem Res. 2011; 44:853–862. [PubMed: 21528865]

231. Kitamura N, Kosuda S, Araki K, Tomifuji M, Mizokami D, Shiotani A, Shinmoto H, Fujii H, Ichihara K. Comparison of animal studies between interstitial magnetic resonance lymphography

and radiocolloid SPECT/CT lymphoscintigraphy in the head and neck region. Ann Nucl Med. 2012; 26:281–285. [PubMed: 22237675]

232. Torres Martin de Rosales R, Tavare R, Glaria A, Varma G, Protti A, Blower PJ. ((9)(9)m)Tc-bisphosphonate-iron oxide nanoparticle conjugates for dual-modality biomedical imaging. Bioconjug Chem. 2011; 22:455–465. [PubMed: 21338098]
233. Patel N, Duffy BA, Badar A, Lythgoe MF, Arstad E. Bimodal imaging of inflammation with SPECT/CT and MRI using Iodine-125 labeled VCAM-1 targeting microparticle conjugates. Bioconjug Chem. 2015; 26:1542–1549. [PubMed: 26218622]
234. Zolata H, Abbasi Davani F, Afarideh H. Synthesis, characterization and theranostic evaluation of Indium-111 labeled multifunctional superparamagnetic iron oxide nanoparticles. Nucl Med Biol. 2015; 42:164–170. [PubMed: 25311750]
235. Wang H, Kumar R, Nagesha D, Duclos RI Jr, Sridhar S, Gatley SJ. Integrity of (111)In-radiolabeled superparamagnetic iron oxide nanoparticles in the mouse. Nucl Med Biol. 2015; 42:65–70. [PubMed: 25277378]
236. Tang Y, Zhang C, Wang J, Lin X, Zhang L, Yang Y, Wang Y, Zhang Z, Bulte JW, Yang GY. MRI/SPECT/Fluorescent Tri-modal probe for evaluating the homing and therapeutic efficacy of transplanted mesenchymal stem cells in a rat ischemic stroke model. Adv Funct Mater. 2015; 25:1024–1034. [PubMed: 26290659]
237. Chen J, Zhu S, Tong L, Li J, Chen F, Han Y, Zhao M, Xiong W. Superparamagnetic iron oxide nanoparticles mediated (131)I-hVEGF siRNA inhibits hepatocellular carcinoma tumor growth in nude mice. BMC Cancer. 2014; 14:1–8. [PubMed: 24383403]
238. Park SI, Kwon BJ, Park JH, Jung H, Yu KH. Synthesis and characterization of 3-[131I]iodo-L-tyrosine grafted Fe3O4@SiO2 nanocomposite for single photon emission computed tomography (SPECT) and magnetic resonance imaging (MRI). J Nanosci Nanotechnol. 2011; 11:1818–1821. [PubMed: 21456300]
239. Ai F, Ferreira CA, Chen F, Cai W. Engineering of radiolabeled iron oxide nanoparticles for dual-modality imaging. Wiley Interdiscip Rev Nanomed Nanobiotechnol. 2015; 22:619–630.
240. Glaus C, Rossin R, Welch MJ, Bao G. In vivo evaluation of (64)Cu-labeled magnetic nanoparticles as a dual-modality PET/MR imaging agent. Bioconjug Chem. 2010; 21:715–722. [PubMed: 20353170]
241. Jarrett BR, Gustafsson B, Kukis DL, Louie AY. Synthesis of 64Cu-labeled magnetic nanoparticles for multimodal imaging. Bioconjug Chem. 2008; 19:1496–1504. [PubMed: 18578485]
242. Lee HY, Li Z, Chen K, Hsu AR, Xu C, Xie J, Sun S, Chen X. PET/MRI dual-modality tumor imaging using arginine-glycine-aspartic (RGD)-conjugated radiolabeled iron oxide nanoparticles. J Nucl Med. 2008; 49:1371–1379. [PubMed: 18632815]
243. Xie J, Chen K, Huang J, Lee S, Wang J, Gao J, Li X, Chen X. PET/NIRF/MRI triple functional iron oxide nanoparticles. Biomaterials. 2010; 31:3016–3022. [PubMed: 20092887]
244. Yang X, Hong H, Grailer JJ, Rowland IJ, Javadi A, Hurley SA, Xiao Y, Yang Y, Zhang Y, Nickles RJ, Cai W, Steeber DA, Gong S. cRGD-functionalized, DOX-conjugated, and (6)(4)Cu-labeled superparamagnetic iron oxide nanoparticles for targeted anticancer drug delivery and PET/MR imaging. Biomaterials. 2011; 32:4151–4160. [PubMed: 21367450]
245. Kim SM, Chae MK, Yim MS, Jeong IH, Cho J, Lee C, Ryu EK. Hybrid PET/MR imaging of tumors using an oleanolic acid-conjugated nanoparticle. Biomaterials. 2013; 34:8114–8121. [PubMed: 23932293]
246. Nahrendorf M, Zhang H, Hembrador S, Panizzi P, Sosnovik DE, Aikawa E, Libby P, Swirski FK, Weissleder R. Nanoparticle PET-CT imaging of macrophages in inflammatory atherosclerosis. Circulation. 2008; 117:379–387. [PubMed: 18158358]
247. Torres Martin de Rosales R, Tavare R, Paul RL, Jauregui-Osoro M, Protti A, Glaria A, Varma G, Szanda I, Blower PJ. Synthesis of 64Cu(II)-bis(dithiocarbamatebisphosphonate) and its conjugation with superparamagnetic iron oxide nanoparticles: in vivo evaluation as dual-modality PET-MRI agent. Angew Chem Int Ed Engl. 2011; 50:5509–5513. [PubMed: 21544908]
248. Cui X, Belo S, Kruger D, Yan Y, de Rosales RT, Jauregui-Osoro M, Ye H, Su S, Mathe D, Kovacs N, Horvath I, Semjeni M, Sunassee K, Szigeti K, Green MA, Blower PJ. Aluminium hydroxide

stabilised MnFe2O4 and Fe3O4 nanoparticles as dual-modality contrasts agent for MRI and PET imaging. Biomaterials. 2014; 35:5840–5846. [PubMed: 24768194]

249. Thorek DL, Ulmert D, Diop NF, Lupu ME, Doran MG, Huang R, Abou DS, Larson SM, Grimm J. Non-invasive mapping of deep-tissue lymph nodes in live animals using a multimodal PET/MRI nanoparticle. Nat Commun. 2014; 5
250. Devaraj NK, Keliher EJ, Thurber GM, Nahrendorf M, Weissleder R. 18F labeled nanoparticles for in vivo PET-CT imaging. Bioconjug Chem. 2009; 20:397–401. [PubMed: 19138113]
251. Sharma R, Xu Y, Kim SW, Schueller MJ, Alexoff D, Smith SD, Wang W, Schlyer D. Carbon-11 radiolabeling of iron-oxide nanoparticles for dual-modality PET/MR imaging. Nanoscale. 2013; 5:7476–7483. [PubMed: 23832243]
252. Choi JS, Park JC, Nah H, Woo S, Oh J, Kim KM, Cheon GJ, Chang Y, Yoo J, Cheon J. A hybrid nanoparticle probe for dual-modality positron emission tomography and magnetic resonance imaging. Angew Chem Int Ed Engl. 2008; 47:6259–6262. [PubMed: 18613191]
253. Hoffman D, Sun M, Yang L, McDonagh PR, Corwin F, Sundaresan G, Wang L, Vijayaragavan V, Thadigiri C, Lamichhane N, Zweit J. Intrinsically radiolabelled [(59)Fe]-SPIONs for dual MRI/radionuclide detection. Am J Nucl Med Mol Imaging. 2014; 4:548–560. [PubMed: 25250204]
254. Wong RM, Gilbert DA, Liu K, Louie AY. Rapid size-controlled synthesis of dextran-coated, 64Cu-doped iron oxide nanoparticles. ACS Nano. 2012; 6:3461–3467. [PubMed: 22417124]
255. Madru R, Tran TA, Axelsson J, Ingvar C, Bibic A, Stahlberg F, Knutsson L, Strand SE. (68)Ga-labeled superparamagnetic iron oxide nanoparticles (SPIONs) for multi-modality PET/MR/Cherenkov luminescence imaging of sentinel lymph nodes. Am J Nucl Med Mol Imaging. 2013; 4:60–69. [PubMed: 24380046]
256. Boros E, Bowen AM, Josephson L, Vasdev N, Holland JP. Chelate-free metal ion binding and heat-induced radiolabeling of iron oxide nanoparticles. Chem Sci. 2015; 6:225–236. [PubMed: 28553472]
257. Pan D, Schmieder AH, Wickline SA, Lanza GM. Manganese-based MRI contrast agents: past, present and future. Tetrahedron. 2011; 67:8431–8444. [PubMed: 22043109]
258. Burtea, C., Laurent, S., Vander Elst, L., Muller, RN. Contrast agents: magnetic resonance. In: Semmler, W., Schwaiger, M., editors. Molecular imaging I. Springer; 2008. p. 135-165.
259. Zhen Z, Xie J. Development of manganese-based nanoparticles as contrast probes for magnetic resonance imaging. Theranostics. 2012; 2:45–54. [PubMed: 22272218]
260. Huang J, Xie J, Chen K, Bu L, Lee S, Cheng Z, Li X, Chen X. HSA coated MnO nanoparticles with prominent MRI contrast for tumor imaging. Chem Commun. 2010; 46:6684–6686.
261. Patel D, Kell A, Simard B, Xiang B, Lin HY, Tian G. The cell labeling efficacy, cytotoxicity and relaxivity of copper-activated MRI/PET imaging contrast agents. Biomaterials. 2011; 32:1167–1176. [PubMed: 21035183]
262. Hu H, Li D, Liu S, Wang M, Moats R, Conti PS, Li Z. Integrin alpha2beta1 targeted GdVO4:Eu ultrathin nanosheet for multimodal PET/MR imaging. Biomaterials. 2014; 35:8649–8658. [PubMed: 25043573]
263. Yoo D, Lee JH, Shin TH, Cheon J. Theranostic magnetic nanoparticles. Acc Chem Res. 2011; 44:863–874. [PubMed: 21823593]
264. Laurent S, Saei AA, Behzadi S, Panahifar A, Mahmoudi M. Superparamagnetic iron oxide nanoparticles for delivery of therapeutic agents: opportunities and challenges. Expert Opin Drug Deliv. 2014; 11:1449–1470. [PubMed: 24870351]
265. Veiseh O, Gunn JW, Zhang M. Design and fabrication of magnetic nanoparticles for targeted drug delivery and imaging. Adv Drug Deliv Rev. 2010; 62:284–304. [PubMed: 19909778]
266. Li C, Li L, Keates AC. Targeting cancer gene therapy with magnetic nanoparticles. Oncotarget. 2012; 3:365–370. [PubMed: 22562943]
267. Cho NH, Cheong TC, Min JH, Wu JH, Lee SJ, Kim D, Yang JS, Kim S, Kim YK, Seong SY. A multifunctional core-shell nanoparticle for dendritic cell-based cancer immunotherapy. Nat Nanotechnol. 2011; 6:675–682. [PubMed: 21909083]
268. Cherukuri P, Glazer ES, Curley SA. Targeted hyperthermia using metal nanoparticles. Adv Drug Deliv Rev. 2010; 62:339–345. [PubMed: 19909777]

269. Kumar CS, Mohammad F. Magnetic nanomaterials for hyperthermia-based therapy and controlled drug delivery. Adv Drug Deliv Rev. 2011; 63:789–808. [PubMed: 21447363]
270. Salunkhe AB, Khot VM, Pawar SH. Magnetic hyperthermia with magnetic nanoparticles: a status review. Curr Top Med Chem. 2014; 14:572–594. [PubMed: 24444167]
271. Thiesen B, Jordan A. Clinical applications of magnetic nanoparticles for hyperthermia. Int J Hyperthermia. 2008; 24:467–474. [PubMed: 18608593]
272. Tassa C, Shaw SY, Weissleder R. Dextran-coated iron oxide nanoparticles: a versatile platform for targeted molecular imaging, molecular diagnostics, and therapy. Acc Chem Res. 2011; 44:842–852. [PubMed: 21661727]
273. Ku G, Zhou M, Song S, Huang Q, Hazle J, Li C. Copper sulfide nanoparticles as a new class of photoacoustic contrast agent for deep tissue imaging at 1064 nm. ACS Nano. 2012; 6:7489–7496. [PubMed: 22812694]
274. Gao D, Zhang P, Liu C, Chen C, Gao G, Wu Y, Sheng Z, Song L, Cai L. Compact chelator-free Ni-integrated CuS nanoparticles with tunable near-infrared absorption and enhanced relaxivity for in vivo dual-modal photoacoustic/MR imaging. Nanoscale. 2015; 7:17631–17636. [PubMed: 26457565]
275. Liu R, Jing L, Peng D, Li Y, Tian J, Dai Z. Manganese (II) chelate functionalized copper sulfide nanoparticles for efficient magnetic resonance/photoacoustic dual-modal imaging guided photothermal therapy. Theranostics. 2015; 5:1144–1153. [PubMed: 26284144]
276. Li Y, Lu W, Huang Q, Huang M, Li C, Chen W. Copper sulfide nanoparticles for photothermal ablation of tumor cells. Nanomedicine (Lond). 2010; 5:1161–1171. [PubMed: 21039194]
277. Tian Q, Jiang F, Zou R, Liu Q, Chen Z, Zhu M, Yang S, Wang J, Wang J, Hu J. Hydrophilic Cu9S5 nanocrystals: a photothermal agent with a 25.7% heat conversion efficiency for photothermal ablation of cancer cells in vivo. ACS nano. 2011; 5:9761–9771. [PubMed: 22059851]
278. Tian Q, Tang M, Sun Y, Zou R, Chen Z, Zhu M, Yang S, Wang J, Wang J, Hu J. Hydrophilic flower-like CuS superstructures as an efficient 980 nm laser-driven photothermal agent for ablation of cancer cells. Adv Mater. 2011; 23:3542–3547. [PubMed: 21735487]
279. Ramadan S, Guo L, Li Y, Yan B, Lu W. Hollow copper sulfide nanoparticle-mediated transdermal drug delivery. Small. 2012; 8:3143–3150. [PubMed: 22829400]
280. Goel S, Chen F, Cai W. Synthesis and biomedical applications of copper sulfide nanoparticles: from sensors to theranostics. Small. 2014; 10:631–645. [PubMed: 24106015]
281. Zhou M, Zhang R, Huang M, Lu W, Song S, Melancon MP, Tian M, Liang D, Li C. A chelator-free multifunctional [64Cu]CuS nanoparticle platform for simultaneous micro-PET/CT imaging and photothermal ablation therapy. J Am Chem Soc. 2010; 132:15351–15358. [PubMed: 20942456]
282. Zhou M, Chen Y, Adachi M, Wen X, Erwin B, Mawlawi O, Lai SY, Li C. Single agent nanoparticle for radiotherapy and radio-photothermal therapy in anaplastic thyroid cancer. Biomaterials. 2015; 57:41–49. [PubMed: 25913249]
283. Zhou M, Zhao J, Tian M, Song S, Zhang R, Gupta S, Tan D, Shen H, Ferrari M, Li C. Radio-photothermal therapy mediated by a single compartment nanoplatform depletes tumor initiating cells and reduces lung metastasis in the orthotopic 4T1 breast tumor model. Nanoscale. 2015; 7:19438–19447. [PubMed: 26376843]
284. Zhou M, Li J, Liang S, Sood AK, Liang D, Li C. CuS Nanodots with Ultrahigh Efficient Renal Clearance for Positron Emission Tomography Imaging and Image-Guided Photothermal Therapy. ACS Nano. 2015; 9:7085–7096. [PubMed: 26098195]
285. Riedinger A, Avellini T, Curcio A, Asti M, Xie Y, Tu R, Marras S, Lorenzoni A, Rubagotti S, Iori M, Capponi PC, Versari A, Manna L, Seregni E, Pellegrino T. Post-synthesis incorporation of (6)(4)Cu in CuS nanocrystals to radiolabel photothermal probes: A feasible approach for clinics. J Am Chem Soc. 2015; 137:15145–15151. [PubMed: 26551614]
286. Liu T, Shi S, Liang C, Shen S, Cheng L, Wang C, Song X, Goel S, Barnhart TE, Cai W, Liu Z. Iron oxide decorated MoS2 nanosheets with double PEGylation for chelator-free radiolabeling and multimodal imaging guided photothermal therapy. ACS Nano. 2015; 9:950–960. [PubMed: 25562533]

287. Cheng L, Shen S, Shi S, Yi Y, Wang X, Song G, Yang K, Liu G, Barnhart TE, Cai W, Liu Z. FeSe2-Decorated Bi2Se3 nanosheets fabricated via cation exchange for chelator-Free Cu-labeling and multimodal image-guided photothermal-radiation therapy. Adv Funct Mater. 2016; 26:2185–2197. [PubMed: 27110230]

288. Gao F, Cai P, Yang W, Xue J, Gao L, Liu R, Wang Y, Zhao Y, He X, Zhao L, Huang G, Wu F, Zhao Y, Chai Z, Gao X. Ultrasmall [(64)Cu]Cu nanoclusters for targeting orthotopic lung tumors using accurate positron emission tomography imaging. ACS Nano. 2015; 9:4976–4986. [PubMed: 25919205]

289. Yang S, Sun S, Zhou C, Hao G, Liu J, Ramezani S, Yu M, Sun X, Zheng J. Renal clearance and degradation of glutathione-coated copper nanoparticles. Bioconjug Chem. 2015; 26:511–519. [PubMed: 25674666]

290. Kotagiri N, Sudlow GP, Akers WJ, Achilefu S. Breaking the depth dependency of phototherapy with Cerenkov radiation and low-radiance-responsive nanophotosensitizers. Nat Nanotechnol. 2015; 10:370–379. [PubMed: 25751304]

291. Hong H, Shi J, Yang Y, Zhang Y, Engle JW, Nickles RJ, Wang X, Cai W. Cancer-targeted optical imaging with fluorescent zinc oxide nanowires. Nano Lett. 2011; 11:3744–3750. [PubMed: 21823599]

292. Rojas S, Gispert JD, Abad S, Buaki-Sogo M, Victor VM, Garcia H, Herance JR. In vivo biodistribution of amino-functionalized ceria nanoparticles in rats using positron emission tomography. Mol Pharm. 2012; 9:3543–3550. [PubMed: 23140442]

293. Shi S, Fliss BC, Gu Z, Zhu Y, Hong H, Valdovinos HF, Hernandez R, Goel S, Luo H, Chen F, Barnhart TE, Nickles RJ, Xu ZP, Cai W. Chelator-Free labeling of layered double hydroxide nanoparticles for in vivo pet imaging. Sci Rep. 2015; 5

294. Zhan Y, Ai F, Chen F, Valdovinos HF, Orbay H, Sun H, Liang J, Barnhart TE, Tian J, Cai W. Intrinsically Zirconium-89 labeled Gd2O2S:Eu nanoprobes for in vivo positron emission tomography and gamma-ray-induced radioluminescence imaging. Small. 2016; 23:201600594.

295. Srivatsan A, Chen X. Recent advances in nanoparticle-based nuclear imaging of cancers. Adv Cancer Res. 2014; 124:83–129. [PubMed: 25287687]

296. Liu TW, MacDonald TD, Shi J, Wilson BC, Zheng G. Intrinsically Copper-64-labeled organic nanoparticles as radiotracers. Angew Chem Int Ed Engl. 2012; 51:13128–13131. [PubMed: 23154923]

297. Liu TW, Macdonald TD, Jin CS, Gold JM, Bristow RG, Wilson BC, Zheng G. Inherently multimodal nanoparticle-driven tracking and real-time delineation of orthotopic prostate tumors and micrometastases. ACS Nano. 2013; 7:4221–4232. [PubMed: 23544841]

298. Huang H, Hernandez R, Geng J, Sun H, Song W, Chen F, Graves SA, Nickles RJ, Cheng C, Cai W, Lovell JF. A porphyrin-PEG polymer with rapid renal clearance. Biomaterials. 2016; 76:25–32. [PubMed: 26517562]

299. Cui L, Lin Q, Jin CS, Jiang W, Huang H, Ding L, Muhanna N, Irish JC, Wang F, Chen J, Zheng G. A PEGylation-free biomimetic porphyrin nanoplatform for personalized cancer theranostics. ACS Nano. 2015; 9:4484–4495. [PubMed: 25830219]

300. Zhang Y, Jeon M, Rich LJ, Hong H, Geng J, Zhang Y, Shi S, Barnhart TE, Alexandridis P, Huizinga JD, Seshadri M, Cai W, Kim C, Lovell JF. Non-invasive multimodal functional imaging of the intestine with frozen micellar naphthalocyanines. Nat Nanotechnol. 2014; 9:631–638. [PubMed: 24997526]

301. Li Y, Lin TY, Luo Y, Liu Q, Xiao W, Guo W, Lac D, Zhang H, Feng C, Wachsmann-Hogiu S, Walton JH, Cherry SR, Rowland DJ, Kukis D, Pan C, Lam KS. A smart and versatile theranostic nanomedicine platform based on nanoporphyrin. Nat Commun. 2014; 5:4712. [PubMed: 25158161]

302. Perez-Medina C, Tang J, Abdel-Atti D, Hogstad B, Merad M, Fisher EA, Fayad ZA, Lewis JS, Mulder WJ, Reiner T. PET imaging of tumor-associated macrophages with 89Zr-labeled high-density lipoprotein nanoparticles. J Nucl Med. 2015; 56:1272–1277. [PubMed: 26112022]

303. Zhang P, Chen Y, Zeng Y, Shen C, Li R, Guo Z, Li S, Zheng Q, Chu C, Wang Z, Zheng Z, Tian R, Ge S, Zhang X, Xia NS, Liu G, Chen X. Virus-mimetic nanovesicles as a versatile antigen-delivery system. Proc Natl Acad Sci USA. 2015; 112:E6129–E6138. [PubMed: 26504197]

304. Lin J, Wang M, Hu H, Yang X, Wen B, Wang Z, Jacobson O, Song J, Zhang G, Niu G, Huang P, Chen X. Multimodal-imaging-guided cancer phototherapy by versatile biomimetic theranostics with UV and gamma-irradiation protection. Adv Mater. 2016; 28:3273–3279. [PubMed: 26928972]

305. Fan Q, Cheng K, Hu X, Ma X, Zhang R, Yang M, Lu X, Xing L, Huang W, Gambhir SS, Cheng Z. Transferring biomarker into molecular probe: melanin nanoparticle as a naturally active platform for multimodality imaging. J Am Chem Soc. 2014; 136:15185–15194. [PubMed: 25292385]

306. Lin X, Xie J, Niu G, Zhang F, Gao H, Yang M, Quan Q, Aronova MA, Zhang G, Lee S, Leapman R, Chen X. Chimeric ferritin nanocages for multiple function loading and multimodal imaging. Nano Lett. 2011; 11:814–819. [PubMed: 21210706]

307. Huang P, Rong P, Jin A, Yan X, Zhang MG, Lin J, Hu H, Wang Z, Yue X, Li W, Niu G, Zeng W, Wang W, Zhou K, Chen X. Dye-loaded ferritin nanocages for multimodal imaging and photothermal therapy. Adv Mater. 2014; 26:6401–6408. [PubMed: 25123089]

308. Ji T, Zhao Y, Wang J, Zheng X, Tian Y, Zhao Y, Nie G. Tumor fibroblast specific activation of a hybrid ferritin nanocage-based optical probe for tumor microenvironment imaging. Small. 2013; 9:2427–2431. [PubMed: 23853124]

309. Wang Z, Huang P, Jacobson O, Wang Z, Liu Y, Lin L, Lin J, Lu N, Zhang H, Tian R, Niu G, Liu G, Chen X. Biomineralization-inspired synthesis of copper sulfide-ferritin nanocages as cancer theranostics. ACS Nano. 2016; 10:3453–3460. [PubMed: 26871955]

310. Huang X, Zhang F, Sun X, Choi KY, Niu G, Zhang G, Guo J, Lee S, Chen X. The genotype-dependent influence of functionalized multiwalled carbon nanotubes on fetal development. Biomaterials. 2014; 35:856–865. [PubMed: 24344357]

311. Goel S, Chen F, Luan S, Valdovinos HF, Shi S, Graves SA, Ai F, Barnhart TE, Theuer CP, Cai W. Engineering intrinsically zirconium-89 radiolabeled self-destructing mesoporous silica nanostructures for in vivo biodistribution and tumor targeting studies. Advanced Science. 2016

312. Munaweera I, Koneru B, Shi Y, Di Pasqua AJ, Balkus J, Kenneth J. Chemoradiotherapeutic wrinkled mesoporous silica nanoparticles for use in cancer therapy. APL Materials. 2014; 2 113315-1-13.

313. Chakravarty R, Goel S, Hong H, Chen F, Valdovinos HF, Hernandez R, Barnhart TE, Cai W. Hollow mesoporous silica nanoparticles for tumor vasculature targeting and PET image-guided drug delivery. Nanomedicine. 2015; 10:1233–1246. [PubMed: 25955122]

314. Song J, Yang X, Jacobson O, Huang P, Sun X, Lin L, Yan X, Niu G, Ma Q, Chen X. Ultrasmall gold nanorod vesicles with enhanced tumor accumulation and fast excretion from the body for cancer therapy. Adv Mater. 2015; 27:4910–4917. [PubMed: 26198622]

315. Lu W, Xiong C, Zhang G, Huang Q, Zhang R, Zhang JZ, Li C. Targeted photothermal ablation of murine melanomas with melanocyte-stimulating hormone analog-conjugated hollow gold nanospheres. Clin Cancer Res. 2009; 15:876–886. [PubMed: 19188158]

316. Cheng B, He H, Huang T, Berr SS, He J, Fan D, Zhang J, Xu P. Gold nanosphere gated mesoporous silica nanoparticle responsive to near-infrared light and redox potential as a theranostic platform for cancer therapy. J Biomed Nanotechnol. 2016; 12:435–449. [PubMed: 26949379]

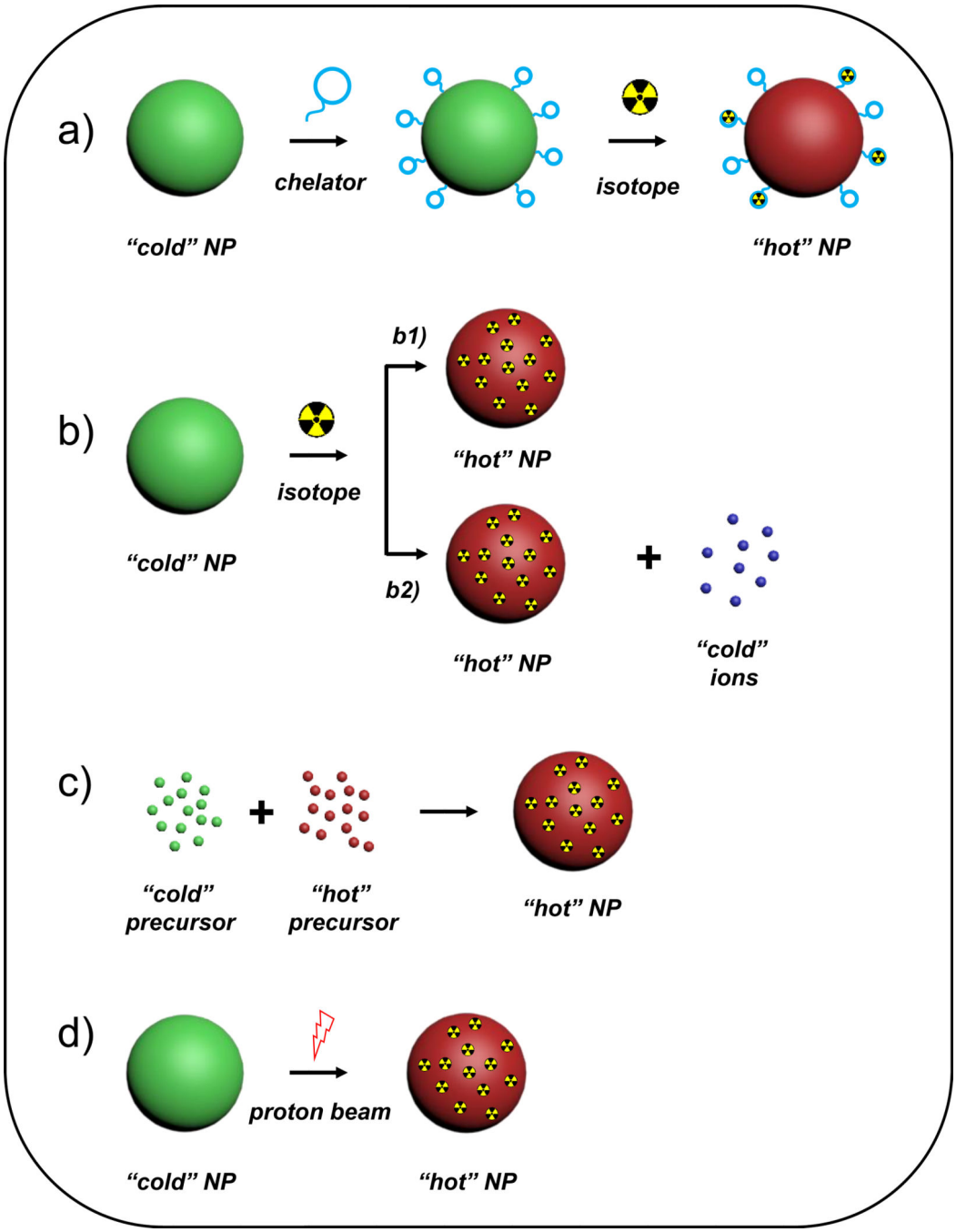

Figure 1.

Schematics depicting five major strategies for radiolabeling nanomaterials. (**a**) Chelator-mediated complexation, (**b**) Specific trapping (**b1**) and ion-exchange (**b2**). (**c**) Hot-plus-cold precursor synthesis, (**d**) Proton beam activation. NP: nanoparticle.

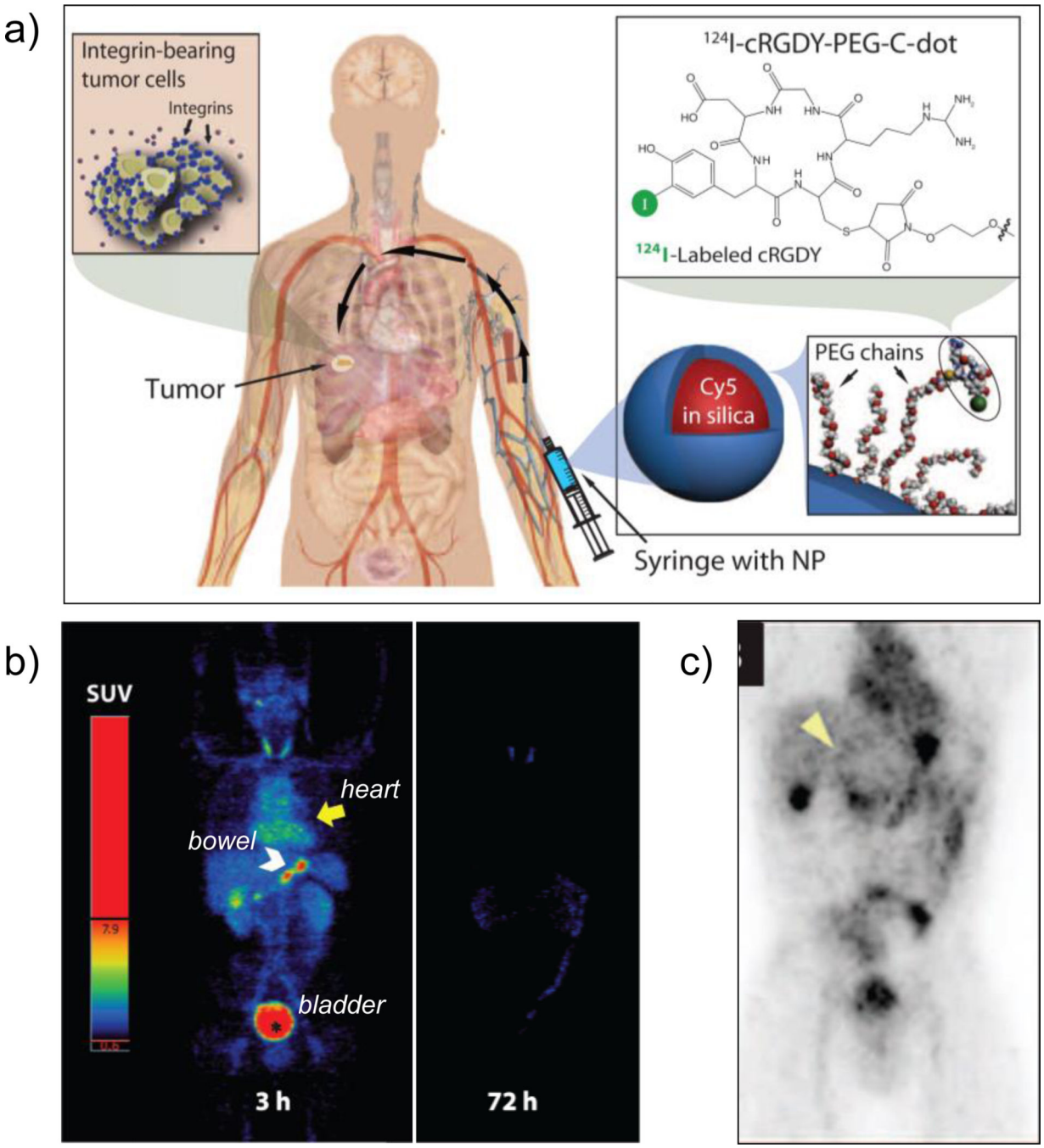

Figure 2.

(**a**) Schematic of the IND-approved hybrid (PET-optical) imaging nanoparticles (C dots). The core-contains Cy5 dye and the surface was attached with poly(ethylene glycol) (PEG) chains, integring $\alpha_v\beta_3$-binding cRGDY peptide ligands and ^{124}I radiolabel. (**b**) Maximum intensity PET projections, 3 and 72 h after intravenous injection of ^{124}I-cRGDY–PEG–C dots. (**c**) Coronal PET image 4 h p.i., demarcating the peripheral aspect of the tumor (arrowhead) and other major organs of nanoparticle uptake (bladder, gastro-intestina tract,

gall bladder and heart). Adapted with permission from [36]. Copyright by American Association for the Advancement of Science.

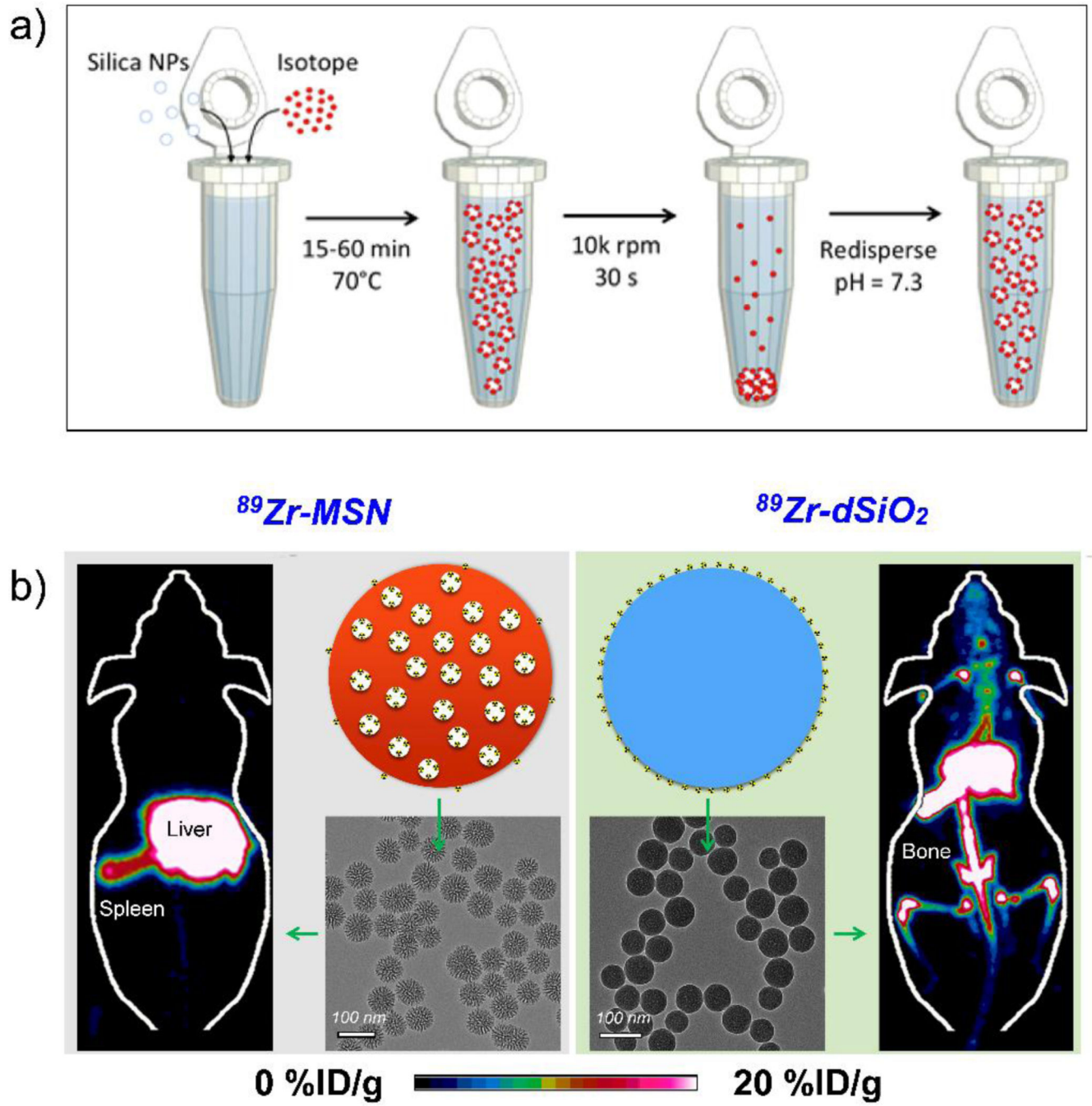

Figure 3.

(**a**) Scheme for intrinsic radiolabeling of silica nanoparticles; incubation of the nanoparticles with free isotope at 70°C for 15–60 min, followed by purification by centrifugation. Adapted with permission from [22] (**b**) Maximum intensity projection PET image, schematic and Transmission electron microscopy (TEM) images of ^{89}Zr-labeled mesoporous silica (^{89}Zr-MSN) (left) and ^{89}Zr-labeled dense silica (^{89}Zr-$dSiO_2$) (right). Absence of radioacitivity from the bones in the case of ^{89}Zr-MSN demonstrates the high *in vivo* radiostability of these

intrinsically radiolabeled nanoparticles when compared with that of ^{89}Zr-dSiO_2. Reproduced with permission from [23]. Copyright by American Chemical Society.

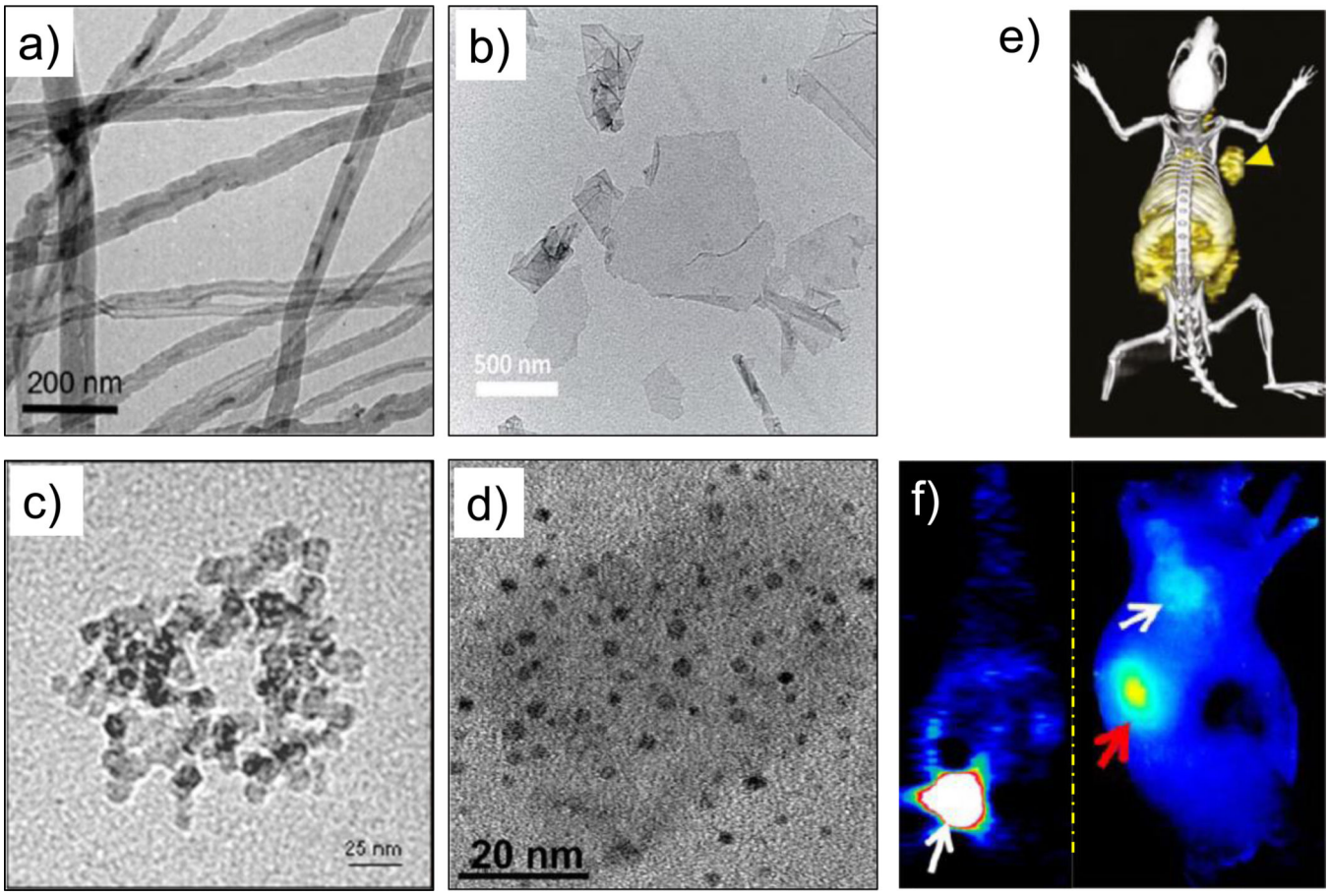

Figure 4.

TEM images of different (radiolabeled) carbon nanomaterials. (**a**) ^{14}C-labeled multiwalled carbon nanotubes. Adapted with permission from [77]. Copyright by American Chemical Society. (**b**) Graphene oxide nanosheets. Adapted with permission from [95]. Copyright of the Royal Society of Chemistry. (**c**) Amine-modified nanodiamonds. Adapted with permission from [62]. (**d**) 800ZW-conjugated carbon nanodots. Adapted with permission from [98]. (**e**) *In vivo* PET/CT image of ^{64}Cu-labeled GO conjugates in 4T1 murine breast tumor-bearing mice. Adapted with permission from [88]. (**f**) Coronal PET image 1 h p.i. of renal clearable ^{64}Cu-labeled carbon nanodots; bladder indicated by white arrow (left), and NIR fluorescence image of SSC-7 tumor-bearing mice, 2 h p.i. of 800ZW-carbon nanodots; white arrow indicates the tumor and red arrow kidney (right). Adapted with permission from [98]. Copyright by American Chemical Society.

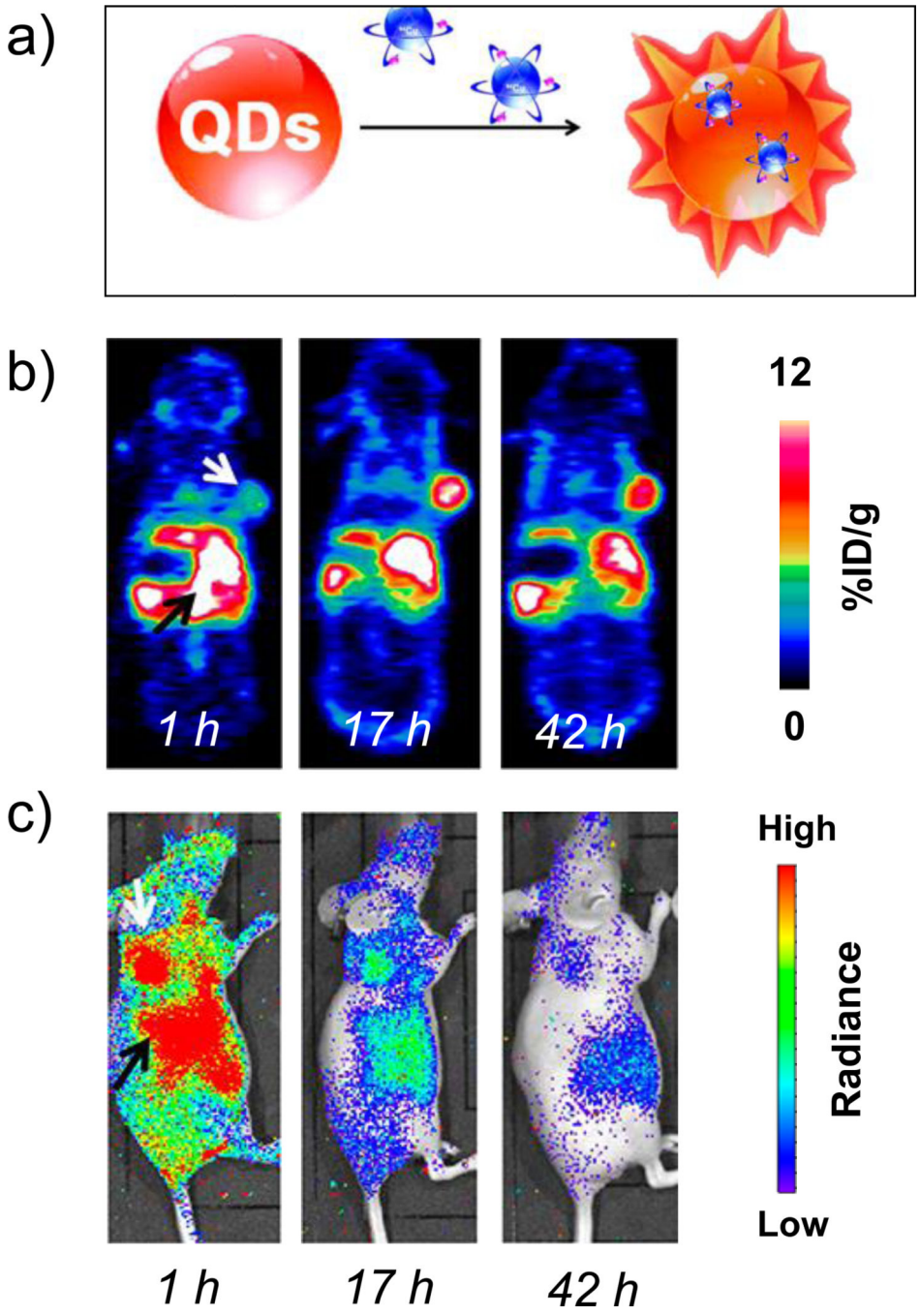

Figure 5.

(**a**) Schematic of self-illuminating ^{64}Cu-doped quantum dots. Representative whole-body (**b**) coronal PET images, and (**c**) luminescence images, of U87MG tumor-bearing mice at 1, 17, and 42 h after intravenous injection of ^{64}Cu-doped QD580. White arrow:tumor area; black arrow:liver area. Adapted with permission from [28]. Copyright by American Chemical Society.

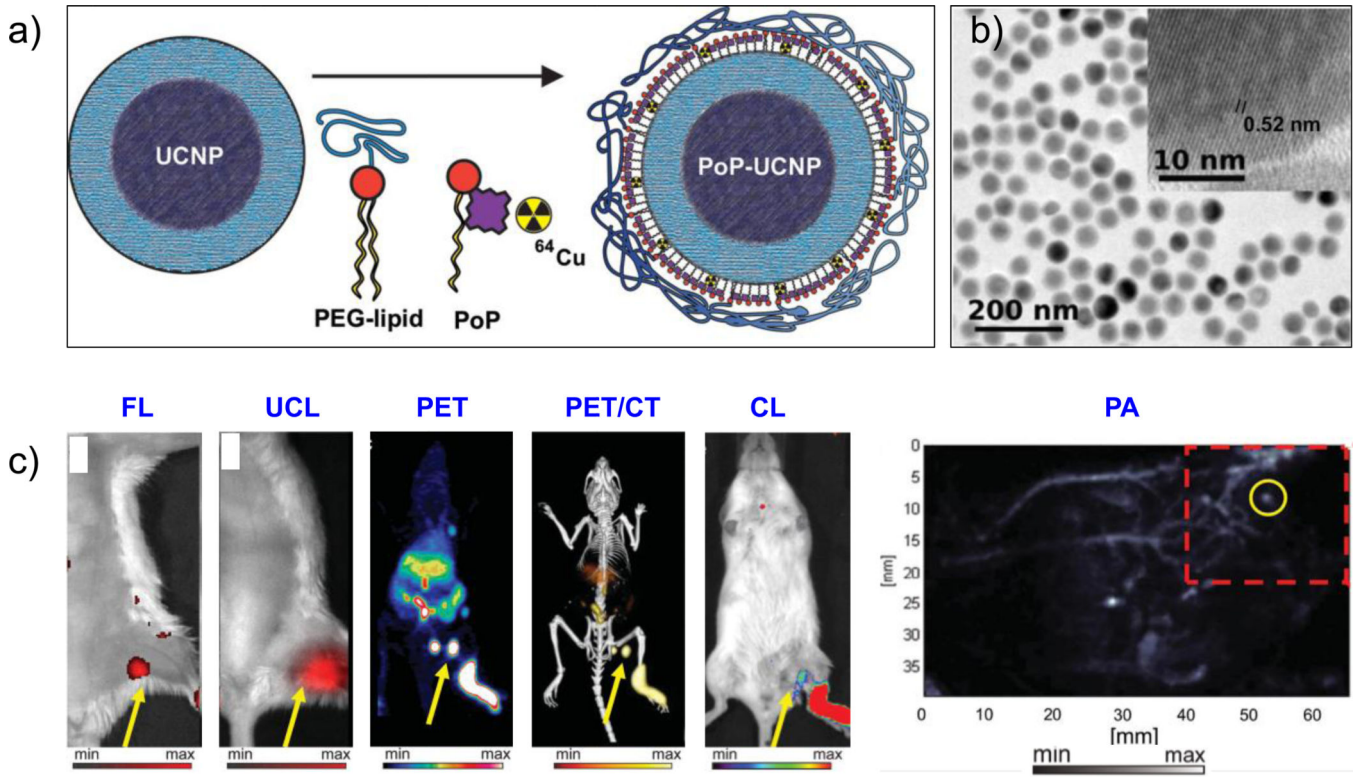

Figure 6.

(**a**) Schematic diagram of the PoP-UCNP structure. Core-shell UCNPs were transferred to the aqueous phase by lipid coating with PEG-lipid and porphyrin-phospholipid (PoP) followed by seamless intrinsic radiolabeling with ^{64}Cu. (**b**) TEM image of PoP-UCNP, with the inset showing the crystalline and core-shell nanostructure of UCNP. (**c**) Hexamodal *in vivo* lymphatic imaging using PoP-UCNPs in mice *via* fluorescence imaging (FL), upconversion luminescence (UCL) imaging, PET, PET/CT, Cerenkov luminescence (CL) imaging, and photoaccoustic (PA) imaging. Reproduced with permission from [140]. Copyright by John Wiley and Sons.

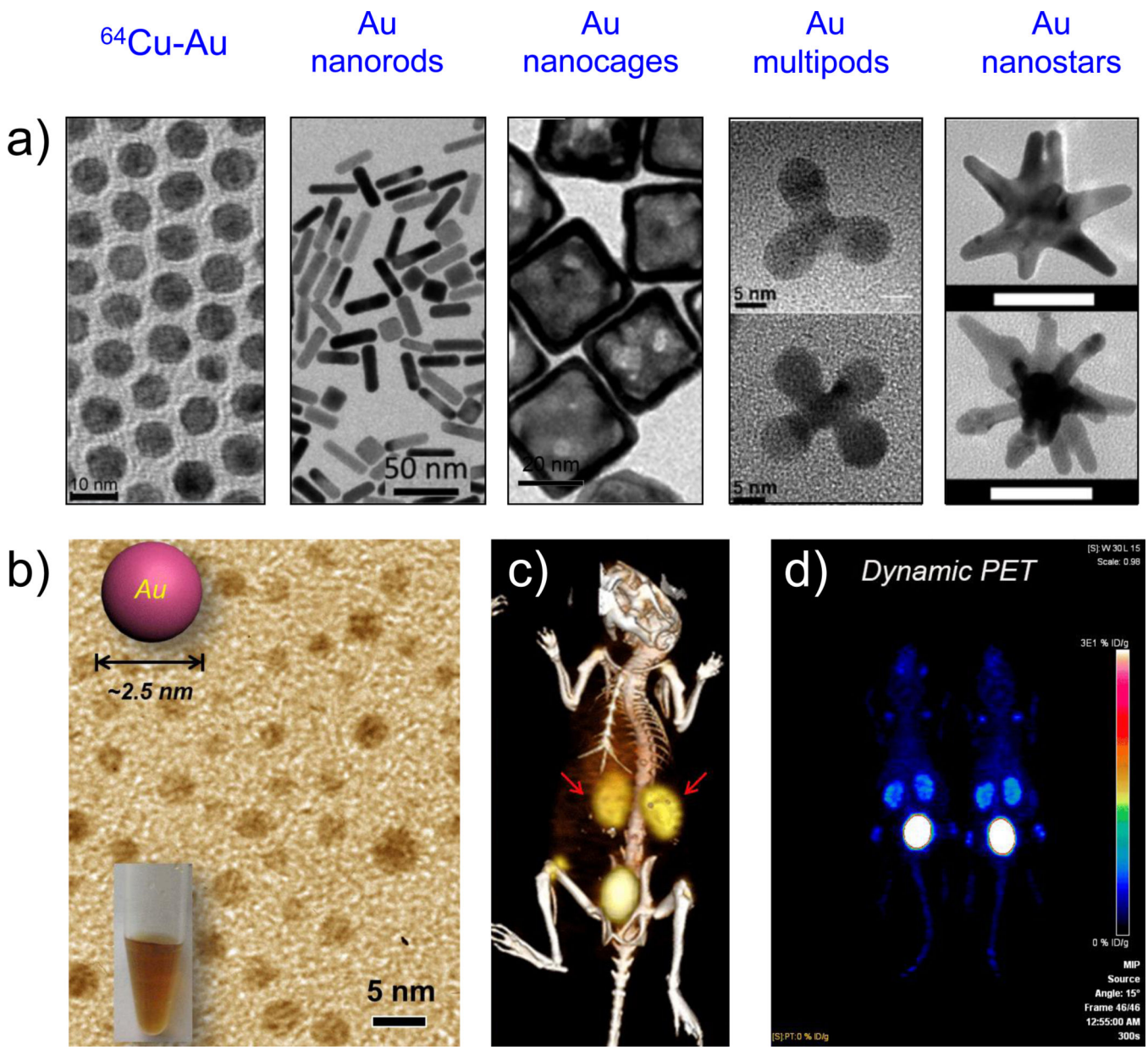

Figure 7.

(**a**) TEM images of various morphologies of gold nanoparticles. From left to right: Alloyed ^{64}Cu-Au nanoparticles. Adapted with permission from [213]; Copyright by John Wiley and Sons. Au nanorods. Adapted with permission from [212]. Au nanocages. Adapted with permission from [1[201]. Au multipods; upper panel, tripod; lower panel, tetrapod. Adapted with permission from [203]. Copyright by American Chemical Society. Au nanostars. Adapted with permission from [180]. Copyright of Multidisciplinary Digital Publishing Institute. (**b**) TEM image of 2–3 nm sized renal clearable ultrasmall gold nanoparticles. (**c**) Representative PET/CT image of mouse injected with ^{64}Cu-NOTA-Au-GSH, 2 h p.i. Kidneys are marked by the red arrow. (**d**) Selected frame (55 min p.i.) from

dynamic PET scanning of ^{64}Cu-NOTA-Au-GSH. Adapted with permission from [206]. Copyright by John Wiley and Sons.

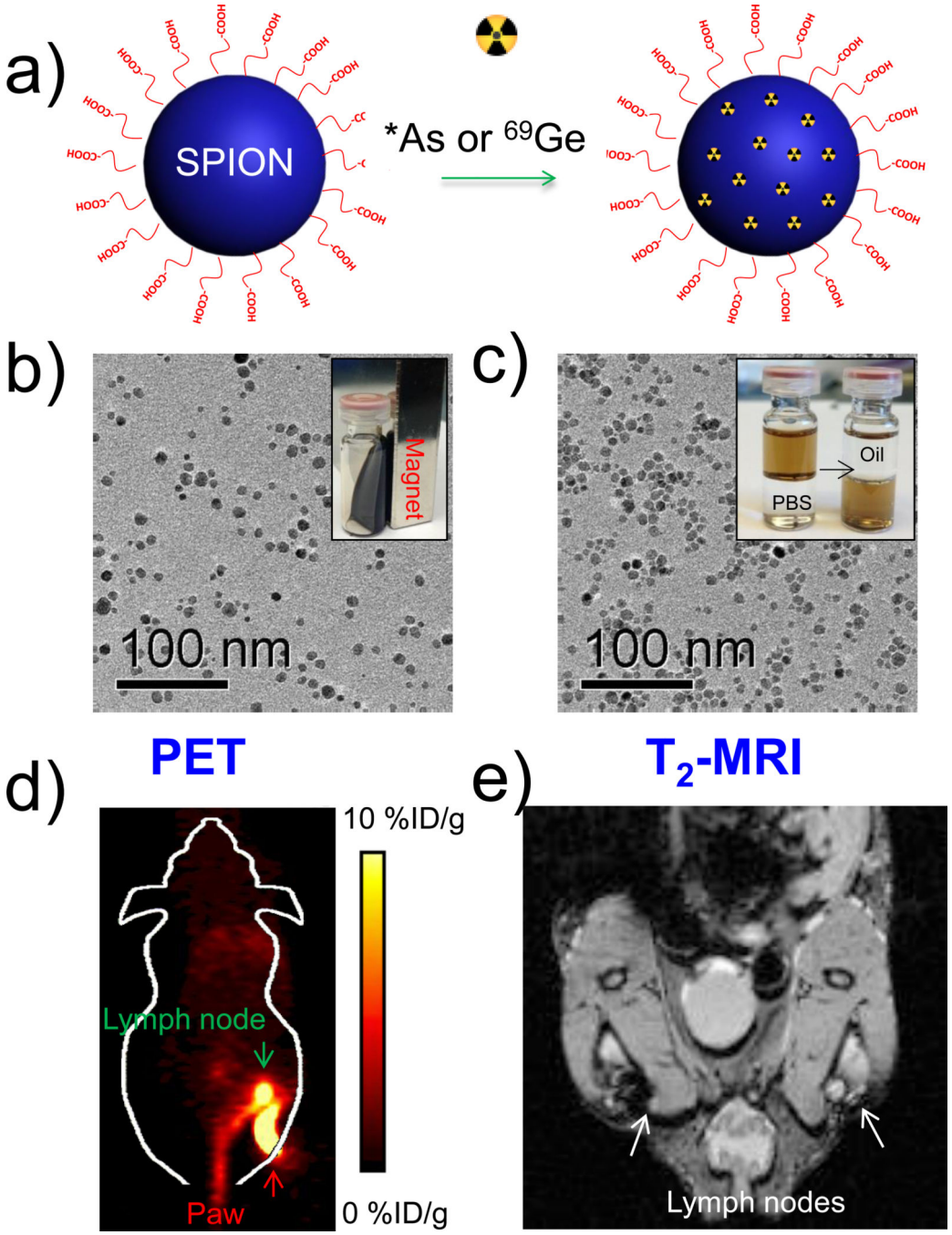

Figure 8.

(**a**) Schematic illustration of chelator-free synthesis of *As (Or ^{69}Ge)-SPION. **(b)** TEM image of oleic acid capped SPIONs (SPIONOA); inset shows the ferrofluidic behavior of SPIONOA. **(c)** TEM image of poly(acrylic acid)-modified SPIONs (SPIONPAA);inset depicts transfer of the SPIONs from oil phase to water phase. **(d)** In vivo lymph node PET imaging 2.5 h after subcutaneous injection of *As-SPIONPEG. **(e)** In vivo MR lymph node mapping 15 h post injection of SPIONPAA into the left footpad of the mouse. Adapted with permission from [24]. Copyright by John Wiley and Sons.

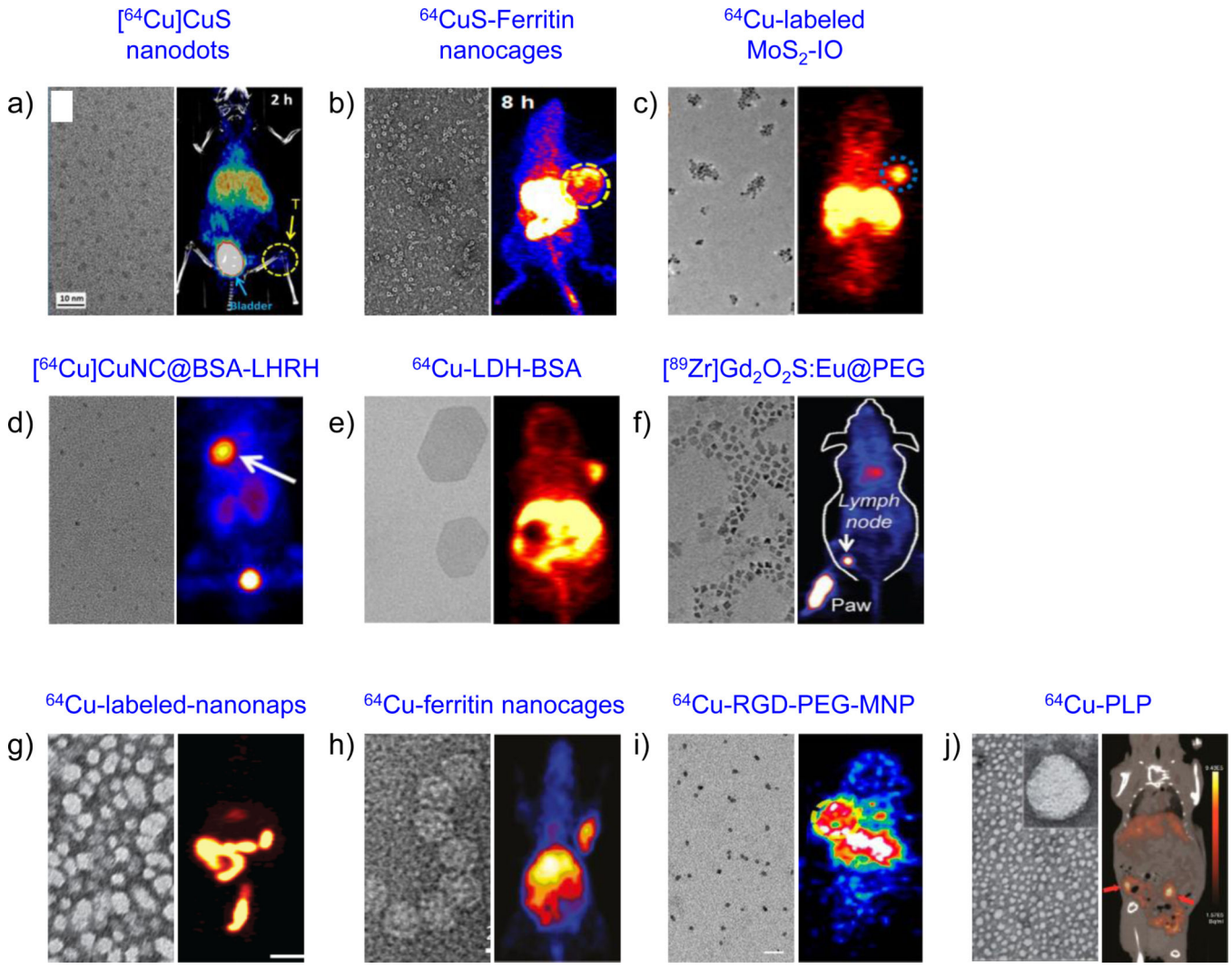

Figure 9.

Representative examples of other inorganic (**a–f**) and organic (**g–j**) nanomaterials employed for PET-guided cancer theranostics. Left panel: TEM images, right panel: in vivo PET images. (**a**) Copper sulfide nanodots; PET/CT image depicts 4T1 tumor uptake (yellow arrow) and dominant renal clearance (blue arrow; bladder) after i.v. injection of 5.6 nm sized [^{64}Cu]CuS nanodots. Reproduced with permission from [284]. (**b**) Biomimetic CuS-Ferritin nanocages. TEM image depicts a dark CuS core inside a ferritin cage and PET image shows U87MG tumors (yellow circle), 8 h after i.v. injection of ^{64}CuS-Ferritin nanocages. Reproduced with permission from [309]. (**c**) Iron oxide decorated MoS_2 nanosheets. TEM image shows double-PEGylated MoS_2-IO and PET image shows enhanced EPR-mediated uptake of intrinsically ^{64}Cu-labeled MoS_2-IO in 4T1 tumor-bearing mice (blue circle), 24 h p.i. Reproduced with permission from [286]. (**d**) High resolution TEM image of ultrasmall BSA-coated Cu nanoclusters (CuNCBSA). PET image depicts LHRH peptide-aided uptake of [^{64}Cu]CuNCBSA-LHRH in orthotopic A549 lung tumor bearing mice (white arrow). Reproduced with permission from [288]. Copyright of American Chemical Society. (**e**) Layered double hydroxide (LDH) nanoparticles. Coronal PET image 16 h p.i. of ^{64}Cu-LDH-

BSA shows enhanced 4T1 tumor uptake. Reproduced with permission from [293]. Copyright of Nature Publishing Group. (**f**) TEM image shows Gd_2O_2S:Eu nanoparticles before PEGylation. PET-based lymph node mapping shows rapid delineation of sentinel lymph nodes 0.5 h after injection of [^{89}Zr]Gd_2O_2S:EuPEG nanoparticles. Reproduced with permission from [294]. Copyright of John Wiley and Sons. (**g**) TEM image of ~20 nm frozen naphthalocyanine micelles (nanonaps) and PET image of ^{64}Cu-labeled-nanonaps, 3 h after oral gavage. Reproduced with permission from [300]. Copyright of Nature Publishing Group. (**h**) TEM image of hybrid ferritin nanocages, conjugated to RGD targeting moiety and Cy5.5 dye. PET images of cRGDyK targeting of U87MG tumors, 24 h after the administration of ferritin nanoprobes. Reproduced with permission from [306]. (**i**) TEM image of multimodal PEGylated melanin nanoparticles (MNP; 10.7 nm) and PET images of ^{64}Cu-RGD-PEG-MNP in U87MG tumor-bearing mice, 24 h p.i. Reproduced with permission from [305] (**j**) TEM shows a core-shell spherical structure of porphylipoprotein (PLP). PET/CT image of mouse with ovarian cancer metastasis after 24 h intravenous injection of ^{64}Cu-PLP (red arrow: tumor). Reproduced with permission from [299]. Copyright of American Chemical Society.

Table 1

Representative Radiolabeled Theranostic Nanoparticles

Class	Nanoparticle	Isotope	Therapeutic Arm	Reference
Silica	MSN	^{64}Cu	Drug Delivery	[43–45]
		^{135}Ho	Chemotherapy, RT	[312]
	HMSN	^{64}Cu	Drug Delivery	[55, 313]
	Biodegradable MSN	^{89}Zr	Drug Delivery	[311]
Carbon	SWNT	Na^{125}I	RIT	[82]
		^{225}Ac	RIT	[83]
		^{89}Zr/^{225}Ac	RIT	[80]
	Graphene Oxide	^{64}Cu	PDT	[85]
Gold	Nanostars	^{131}I	PTT	[181]
	Nanorod Vesicles	^{64}Cu	PTT	[314]
	Nanorods	^{64}Cu	PTT	[21]
			Drug Delivery	[202]
		^{125}I	PTT	[191]
	Nanoshells	^{18}F	PTT	[315]
Magnetic	SPION	^{64}Cu	Drug Delivery	[244]
		^{131}I	Gene Therapy	[237]
		^{111}In	Chemotherapy	[234]
Copper Sulfide	Nanospheres	^{64}Cu	PTT	[17, 281]
			RT, PTT	[282, 283]
	Nanodots	^{64}Cu	PTT	[284]
Porphyrin	Porphylipoprotein	^{64}Cu	PDT, Drug Delivery	[299]
	Nanoporphyrin	^{64}Cu	PDT, PTT, Drug Delivery	[301]

RT = Radiotherapy, RIT = Radioimmunotherapy, PDT = Photodynamic Therapy, PTT = Photothermal Therapy,

Table 2

Selected Multi-component Radiolabeled Nanoparticle Systems

Component 1	Component 2	Imaging Modality	Therapeutic Modality	References
Silica	Gold Nanoshell	PET	−/−	[192, 193]
		PET	PTT	[194]
	Gold Nanosphere	PET	Chemotherapy, PTT	[316]
SPION	Silica	PET/MR	−/−	[34, 35]
		SPECT/MR	−/−	[238]
		SPECT/MR/FL	Stem Cell Therapy	[236]
	Gold	PET/MR/FL	−/−	[204]
	$Al(OH)_3$	PET/MR	−/−	[248]
	Crosslinked Dextran	PET/CT	−/−	[250]
	Melanin	PET/MR/PAT/PTI	PTT	[304]
QDs	Phospholipid Micelles	PET/FL	−/−	[112]
UCNP	Porphyrin phospholipid	PET/PA/FL/UCL/CT/Cerenkov	−/−	[140]
	Micelle	PET/UCL	−/−	[139]
Graphene	Gold Nanorod Vesicle	PET/PAT	PT, Drug Delivery	[96]
	SPION	PET/MR/PAT	−/−	[89]
CuS	Silica	PET	PTT	[33]
	Ferritin	PET/PAT	PTT	[309]
MoS_2	SPION	PET/PAT/MR	PTT	[286]
Bi_2Se_3	$FeSe_2$	PET/CT/MR/PAT	PTT, RT	[287]

PTI = Photothermal Imaging, PAT = Photoacoustic Tomography